



Published in final edited form as:

Nanotoxicology. 2019 November ; 13(9): 1176–1196. doi:10.1080/17435390.2019.1645903.

Single-walled Carbon Nanotubes Repress Viral-Induced Defense Pathways through Oxidative Stress

Hao Chen[†], Sara T. Humes[†], Sarah E. Robinson[†], Julia C. Loeb[†], Indu V. Sabaraya[‡], Navid B. Saleh[†], Ram B. Khattri[#], Matthew E Merritt[#], Christopher J. Martyniuk^{*}, John A. Lednicky[†], Tara Sabo-Attwood[†]

[†]Department of Environmental and Global Health, Center for Environmental and Human Toxicology and Emerging Pathogens Institute, University of Florida, Gainesville, FL, 32611, USA;

[‡]Department of Department of Civil, Architectural, and Environmental Engineering, University of Texas Austin, Austin, TX, 78712, USA;

[#]Department of Biochemistry & Molecular Biology, University of Florida, Gainesville, FL, 32610, USA;

^{*}Department of Physiological Sciences and Center for Environmental and Human Toxicology, University of Florida, Gainesville, FL, 32611, USA

Abstract

Exposure of lung cells *in vitro* or mice to single-walled carbon nanotubes (SWCNTs) directly to the respiratory tract leads to a reduced host anti-viral immune response to infection with influenza A virus H1N1 (IAV), resulting in significant increases in viral titers. This suggests that unintended exposure to nanotubes via inhalation may increase susceptibility to notorious respiratory viruses that carry a high social and economic burden globally. However, the molecular mechanisms that contribute to viral susceptibility have not been elucidated. In the present study, we identified the retinoic acid-induced gene I (RIG-I) like receptors (RLRs)/mitochondrial antiviral signaling (MAVS) pathway as a target of SWCNT-induced oxidative stress in small airway epithelial cells

Corresponding Author: Tara Sabo-Attwood, PhD, Center for Environmental and Human Toxicology, Department of Environmental and Global Health, University of Florida, Box 110885, 2187 Mowry Road, Gainesville, FL 32611. sabo@phhp.ufl.edu; Phone: 3522945293.

Author contributions

The manuscript was prepared through contributions of all authors. TSA, JAL, NSB, HC, CM conceived and designed the experiments. HC, STH, SER, JCL, IVS performed the experiments. HC, IVS, and TSA analyzed the data and prepared the figures. HC, IVS and TSA wrote and revised the manuscript. All authors read and approved the final manuscript.

Supplemental information

Methods on Nuclear Magnetic Resonance on SAEC and autophagy test in SAEC, supplemental table 1 (leached metal concentrations in media), supplemental table 2 (primer information), supplemental table 3 (compounds identified from NMR assay), supplemental figure 1 (HDR of SWCNTs in RPMI media), supplemental figure 2 (expression level comparison of immune genes), supplemental figure 3 (time-course changes of ROS by SWCNTs).

Ethics approval and consent to participate

Not applicable

Consent for publication

Not applicable

Availability of data and material

All data generated or analyzed during this study are included in this published article.

Competing interests

The authors declare no competing interests.

(SAEC) that contribute to significantly enhanced influenza viral titers. Exposure of SAEC to SWCNTs increases viral titers while repressing several aspects of the RLR pathway, including mRNA expression of key genes (e.g. *IFITs*, *RIG-I*, *MDA5*, *IFN β 1*, *CCL5*). SWCNTs also reduce mitochondrial membrane potential without altering oxygen consumption rates. Our findings also indicate that SWCNTs can impair formation of MAVS prion-like aggregates, which is known to impede downstream activation of the RLR pathway and hence the transcriptional production of interferon-regulated anti-viral genes and cytokines. Furthermore, application of the antioxidant NAC alleviates inhibition of gene expression levels by SWCNTs, as well as MAVS signalosome formation, and increased viral titers. These data provide evidence of targeted impairment of anti-viral signaling networks that are vital to immune defense mechanisms in lung cells, contributing to increased susceptibility to IAV infections by SWCNTs.

Keywords

single-walled carbon nanotubes; influenza A virus; oxidative stress; infection; innate immune response

Introduction

Carbon nanotubes (CNTs) have been widely used in commercial and industrial sectors due to their unique physical and chemical properties, which allow for modifications that are ideal for product development (Martin & Kohli, 2003). Products that contain CNTs have continued to grow, and one report estimates that the worldwide production of CNTs will reach \$3.42 billion by 2022 (GRV, 2015). Increasing use of CNTs in a variety of applications raises concerns over their potential exposure and subsequent toxic effects, particularly through the route of inhalation, because of their nanometer size and proposed accessibility to the deeper airways. Epidemiological studies have reported significant airborne levels of CNTs in occupational settings (Dahm et al., 2018), and blood samples from exposed workers had elevated levels of early toxicity biomarkers related to oxidative stress and pulmonary fibrosis (Beard et al., 2018; Liao et al., 2014).

Most toxicology studies focus on the health effects associated with exposure to single environmental chemicals, but fewer have considered how exposure to small particulates, such as CNTs, impact host susceptibility to infectious agents. Several lines of evidence report that worsened health is associated with exposure to multiple stressors that include chemicals and pathogens. For example, exposure to both aflatoxin and hepatitis B virus (HBV) together leads to 59.4 times higher risk of developing liver cancer compared to only 7.3 and 3.4 times the risk for HBV or aflatoxin exposure alone (Groopman et al, 2005; Qian et al., 1994). In addition, exposure to particulates (i.e. diesel exhaust, cigarette smoke) can modulate immune responses that are associated with increased risk of respiratory infections by viruses (Duffney et al., 2018; Gowdy et al., 2010; Jaspers et al., 2009).

In terms of CNTs, we have focused on SWCNTs because they tend to show high toxicity and in many cases are not degraded and/or cleared as readily as other types in cells or tissues (i.e. functionalized SWCNTs, MWCNTs) (Kotchey et al., 2012; Park et al., 2016; Qin et al., 2017; Sturm, 2014). Studies report that exposure to single-walled carbon nanotubes

(SWCNTs) exacerbated pulmonary inflammation and hindered bacterial clearance in the respiratory system of mice (Shvedova et al., 2008; Shvedova et al., 2005; Walling et al., 2013). In a recent study, our group first reported that exposure to SWCNTs increased influenza A virus (IAV) titers 5 fold in small airway epithelial cells (SAEC) while modulating key genes that are important for viral replication and inflammatory responses, such as interferon induced protein with tetratricopeptide repeats 2 and 3 (IFIT2 and IFIT3) (Sanpui et al., 2014). This enhanced production of infectious IAV particles was more prominent in a mouse model, where exposure to SWCNTs followed by IAV infection led to virus titers in the lung that were 63 times higher compared to virus exposure alone (Chen et al., 2017). These mice also presented with exacerbated inflammation and more severe pneumonia in the co-exposure group (Chen et al., 2017). Importantly, we also noted that a comparable carbon black control particle did not elicit enhanced viral titers (Sanpui et al., 2014), nor did exposure to a functionalized multi-walled carbon nanotubes (unpublished data). Though these observations are novel and significant, little is known about the mechanisms of how SWCNTs elicit these responses at the molecular level.

A primary mechanism of CNT-mediated toxicity that has been well reported in the literature is the induction of oxidative stress characterized by reactive oxygen species (ROS) production and activation of redox-cycling pathways (Dong & Ma, 2016; Shvedova et al., 2009). A major source and target of oxidative stress is the mitochondria, which not only produces ATP, but also houses several antiviral signaling proteins critical for innate immune signaling; these include mitochondrial antiviral signaling proteins (MAVSs). MAVS is central to activation of the retinoic acid induced-gene I-like receptors (RLRs) innate antiviral signaling pathway, and its regulation is largely dependent on mitochondrial structure and function (Jacobs et al., 2014). RLRs (including RIG-I, melanoma differentiation-associated protein 5 (MDA5)) are pattern recognition receptors (PRR), a family of proteins that recognize moieties of microbes, including viruses (Hou et al., 2011). Once RIG-I or MDA5 interacts with viral molecules, the formed complex moves to the mitochondria and docks with MAVS aggregates present on the outer mitochondrial membrane to initiate downstream signaling (Hou et al., 2011). While several groups have shown that CNTs produce ROS, no studies have linked this production of oxidative stress to the specific impairment of innate immune pathways involved in viral defense responses that include modulation of RLRs/MAVS signaling. Based on the observation that SWCNTs increased IAV titers and impaired anti-viral gene expression, we hypothesized that these endpoints were triggered by SWCNT-induced ROS, which led to mitochondrial dysfunction through RLRs-MAVS impairment.

Methods

SWCNT suspension preparation and characterization

Pristine SWCNTs (SG65) were purchased from SouthWest Nanotechnologies Inc. (SWeNT, Norman, OK). All SWCNTs were synthesized using a CoMoCAT® chemical vapor deposition (CVD) method, and physicochemical properties, including chirality distribution, morphology, diameter, dispersion coefficients, and metal leaching (primarily cobalt and molybdenum) have previously been reported (Bisesi et al., 2015; Sanpui et al., 2014). Dry

SWCNTs were weighed and added to 1% pluronic F68 solution (v / v in deionized water, Sigma Aldrich, St. Louis, MO) to make a 1 mg/mL working stock suspension and sonicated at 30–50 W for 20 min using Sonifier™ S-450 Sidal Ultrasonic Cell Disruptor/Homogenizer (Branson Ultrasonics, Danbury, CT) in an ice bath. A sample of the SWCNT stock was serially diluted in 1% pluronic and absorbance measured at 775 nm (Synergy H1, Biotek, Winooski, VT). The rest of the stock was centrifuged, and the supernatant was collected and sonicated again for 10 min at 30 W. A sample of the supernatant was also measured for absorbance at 775 nm. The final concentration was calculated using the following equation:

$$[\text{Working solution}] = [\text{Stock}] \times \left[\frac{\text{Absorbance}_{\text{supernatant}}}{\text{Absorbance}_{\text{stock}}} \right]$$

The average hydrodynamic radius (HDR) of the materials in the RPMI media was measured with an ALV/CGS-3 compact goniometer system (ALV-Laser GmbH, Langen/Hessen, Germany), equipped with a 22 mW HeNe 632.8 nm laser. An aliquot of the concentrated stock sample was mixed with the media to achieve a final concentration of 10 mg/L. A volume of 2 mL sample was injected into a pre-cleaned borosilicate glass vial to collect scattered laser intensity at 90° every 30 s for 24 h. A cumulant fit was used to estimate the HDR from scattering intensity. All measurements were conducted at 37 °C. A detailed method has been described elsewhere (Afrooz et al., 2013(a); Khan et al., 2013). Inductively coupled Plasma-optical emission spectroscopy (ICP-OES) methods have been used to detect metal components in SWCNTs. Briefly, samples were acidified with 5% nitric acid, refrigerated for 12 h, and filtered with a 0.2 µm PTFE filter before analyzing for total ionic concentrations using a Varian 720 ICP-OES. Each sample was measured in triplicate. The standard curves achieved R² values of greater than 0.995 from National Institute of Standards and Technology (NIST) certified standard solutions. The electrophoretic mobility (EPM) of the materials was measured using a Malvern Zetasizer (Malvern Instruments Ltd., Worcestershire, UK) at 37 °C. For each measurement, an aliquot of the sample (incubated for 24 h period in the media) was introduced into a disposable capillary cell (DTS 1070, Malvern Instruments Ltd.). The cells were washed with DI water and ethanol between measurements. Measurements were performed in triplicate using a well-established protocol (Afrooz et al., 2013(a); Afrooz et al., 2013(b); Aich et al., 2016).

Cell lines and viability assay

Human SAEC were provided by Dr. Brooke Mossman and were previously characterized by Hei and colleagues (Piao et al., 2005). SAEC were cultured in advanced RPMI 1640 (Life Technologies, Waltham, MA) media with supplementation of 10% (v/v) heat-inactivated or gamma-irradiated fetal bovine serum (FBS) (HyClone, Logan, UT), 1% L-glutaMAX (Gibco, Grand Island, NY), and 1% Penicillin-Streptomycin-Neomycin (PSN) (Gibco, Manassas, VA). All cells were maintained and propagated at 37 °C in a humidified 5% CO₂ incubator.

A trypan blue staining assay was used to determine the viability of SAEC treated with SWCNTs. SAEC were plated in 6-well plates at the density of 3 × 10⁵ per well with

complete RPMI media for 24 h. Then, cells were exposed to different doses of SWCNTs (0.2, 2.0, 20.0, 50.0 µg/mL) suspended in exposure media, which contains advanced RPMI supplemented with 1% L-GlutaMAX and 1% PSN for 24 h. Cells were washed with phosphate buffered saline (PBS) and stained with trypan blue dye (Gibco, Grand Island, NY). Live/dead (blue) cells were differentiated and counted under a light microscope with a hemocytometer. At least 200 cells were counted for each treatment (n = 3) and the entire experiment was repeated 3 times.

Time-course exposure of SAEC to IAV

SAEC were seeded in 6-well plates as described above. After 24 h of incubation, cells were washed with phosphate buffer saline (PBS) and then exposed to influenza virus H1N1 strain A/Mexico/4108/2009 at a multiplicity of infection of 0.5 at 33 °C. Cells were collected at 2, 4, 8, 12, 18, and 24 h post-infection. Control cells were also included at each timepoint. After exposure, cells were collected for gene expression analysis with STAT-60 RNA Extraction Reagent (Tel Test, Friendswood, TX).

SWCNTs and virus co-exposure of lung cells

SAEC were seeded in 6-well plates in complete RPMI media and incubated overnight. Cells were then washed with PBS and exposed to different doses (0.2, 2.0, 20.0, and 50.0 µg/mL) of SWCNTs suspended in exposure RPMI media for 24 h at 37 °C. An equal volume of 1% pluronic as the SWCNT stock was added to cells as controls. After SWCNT exposure, IAV at 0.5 MOI was added to designated wells for another 24 h at 33 °C. Media was collected and used for viral titer assays. The cells were washed with PBS and then collected for gene expression analysis using STAT-60 RNA extraction agent. After RNA extraction, a Synergy H1 Hybrid Reader NanoDrop (Biotek Instruments) was used to determine RNA concentration. Reading was carried out at wavelength 230, 260, 280, and 320 nm, where a 260/280 ratio or 260/230 ratio greater than 1.8 was used to confirm quality and purity of the RNA.

Viral titers by TCID₅₀ assay

Virus particles in the media were quantified by a 50% tissue culture infectious dose (TCID₅₀) assay using endpoint dilutions. Briefly, Madin-Darby Canine Kidney (MDCK) (NBL-2) cells were cultured in Dulbecco Modified Eagle Media (DMEM), supplemented with 10% FBS, 1% L-GlutaMAX, and 1% PSN at 37 °C and seeded in 96-well plates. Serial dilutions (10⁻¹ to 10⁻¹⁰) of virus stock and collected media from SWCNT-IAV co-exposure experiments were added to an MDCK monolayer with addition of N-tosyl-L-phenylalanine chloromethyl ketone (TPCK)-trypsin in the media (8 replicates per dilution). Infected MDCK cells were then incubated at 33 °C for 5 d. The cytopathic effects (CPE) of MDCK monolayers were observed and marked as positive. TCID₅₀, which is defined as the virus dilution required to cause CPE on 50% of multiple inoculated cell batches at a given dilution of the virus, was calculated by the Reed and Muench method (Zamoiskii, 1956).

Expression levels of influenza virus matrix protein 2, innate immune response and oxidative stress genes

STAT-60 collected RNA was extracted using a phenol-chloroform method, quantified, treated with DNase (PerfeCTa DNase I kit, QuantaBio, Beverly, MA) to remove residual genomic DNA, and then reverse transcribed into cDNA (qScript cDNA Synthesis Kit, Beverly, MA). The cDNA was amplified using validated primers (Supp. Tab. 2) and probes specific to each gene target. Expression of *GAPDH* was used for a standard reference gene, and all data except *M2* is presented as normalized fold change in expression compared to controls using Cq method (Livak & Schmittgen, 2001). As control cells show no expression of *M2*, these data at different time-points were normalized as fold change compared to IAV at 2 hours post infection for each experiment. The *M2* fold change was normalized to IAV only in the SWCNTs + IAV experiment. The same gene expression data for the IAV time-course was also graphed as fold change compared to 1 single calibrator (TLR3 control at 2 hours) for the entire gene set. Using this approach enabled us to rank the expression of genes at baseline, and after IAV exposure (at 2 and 24 hours) from lowest to highest expression comparably (Supp. Fig. 2)

Immunofluorescence staining

SAEC were seeded on cover slips in 6-well plates and incubated overnight. Cells were then exposed to SWCNTs and IAV as described earlier. After exposure, cells were incubated with 250 nM mito-tracker red (Invitrogen, Eugene, OR) for 45 min and then fixed with 3.7% PFA for 10 min. The fixed cells were washed with PBS and then treated with ice-cold acetone for 5 min permeabilization. The cells were then incubated with blocking solution (5% goat serum in PBS-Tween buffer) for 1 h. Slides were then incubated with primary mouse anti-MAVS antibody (Santa Cruz, Dallas, TX) at the dilution of 1:200 at 4 °C overnight followed by a 1-h incubation of secondary goat anti-mouse IgG conjugated with FITC (Santa Cruz, Dallas, TX) at 1:1000 dilution at room temperature. Finally, slides were mounted with Fluoroshield Mounting Media with DAPI (Vector, Burlingame, CA) and examined using a Leica TCS-SP5 Confocal Microscope (Wetzlar, Germany).

Measurement of reactive oxygen species production

A 2', 7'-dichlorofluorescein diacetate (DCFDA) Cellular ROS Detection Assay Kit (Abcam, Cambridge, MA) was used to measure the ROS production of SAEC treated with SWCNTs and IAV. According to manufacturer's protocol, about 2×10^4 SAEC cells per well were seeded in black-walled, clear-bottom 96-well microplates and incubated overnight. Cells were then washed and incubated with 25 μ M DCFDA for 45 min following treatment of either SWCNTs (0.2, 2.0, 20.0, 50.0 μ g/mL) or IAV (MOI 0.1, 0.5, 1.0, 5.0) for 4 h. A positive control, 50 μ M H₂O₂, was also included in the experiment. Fluorescence intensity was measured at Excitation / Emission (Ex / Em) = 485 / 535 nm. All readings in the experiment wells were background subtracted and expressed as fold change from control. The assay protocol was modified to test the ROS production in SAEC by SWCNTs-IAV co-exposure. Briefly, SAEC were first exposed to SWCNTs for 24 h followed with IAV exposure for another 24 h. and cells were incubated with 25 μ M DCFDA in media for 45 min and read with fluorescence as described above. In a final experiment cells were exposed

to SWCNTs and IAV, then incubated with and DCFDA and processed for ROS production as described above.

Mitochondrial membrane potential (MMP) assay

A tetramethylrhodamine, ethyl ester (TMRE) MMP Assay kit (Abcam, Cambridge, MA) was used to examine mitochondrial membrane potential impairment by SWCNT and IAV. Based on the manufacturer's protocol, 2×10^4 SAEC cells per well were seeded in 96-well plate and allowed to adhere overnight. Cells were then treated with SWCNTs and IAV as described above. After exposure, a final concentration of 500 nM of TMRE was added to tested cells and incubated for 25 min. The media was then removed and 100 μ L of PBS / 0.2% BSA was used to wash cells twice. The plate was read at Ex / Em = 549 / 575 nm. Wells with SAEC but not treated with TMRE were used as background controls. For the calculation, fluorescence intensity was background subtracted and expressed as fold change from control. Two technical replicates were performed, and the experiment was repeated independently 3 times.

Assessment of mitochondrial bioenergetics

Cellular oxygen consumption rate of SAEC was measured using a Seahorse XFe24 assay (Agilent, Santa Clara, CA). Approximately 2×10^4 SAEC per well were seeded in XFe24 microplates and allowed to adhere overnight. Cells were then exposed to SWCNTs at 0.2, 2.0, 20.0, and 50.0 μ g/mL or control (1% pluronic) for 24 h. Cells were then rinsed twice and incubated in XF mito stress test media (RPMI 1640, 2 mM L-Glutamine, 2 mM sodium pyruvate, 10 mM glucose) at 37 °C in a non-CO₂ incubator. After 45 min, basal respiration rates were measured 3 times followed by injection of oligomycin (final concentration: 1 μ M). Three ATP-associated respiration rates were measured after oligomycin inhibition of ATP synthase, which was then followed by injection of carbonyl cyanide-4 (trifluoromethoxy) phenylhydrazone (FCCP, 1.0 μ M). FCCP can induce maximal oxygen consumption (measured 3 times) by collapsing the mitochondrial proton gradient causing uninhibited electron flow (Sanpui et al., 2014). Finally, antimycin A at the final concentration of 1 μ M was injected to each well to end mitochondrial respiration which allows 3 measurements of non-mitochondrial respiration in the cells. Total protein concentration was used to normalize bioenergetics per well using the Pierce BCA Protein Assay (Thermo Fisher, Waltham, MA). The unit for the data is presented as pmol/ min/mg protein/mL. Mitochondrial bioenergetics data were calculated as per the Seahorse XF Cell Mito Stress Test Kit User Guide (User Guide Kit 103015–100, Agilent): Basal respiration [defined as mean basal OCR measurement], oligomycin induced ATP-linked respiration [defined as (mean basal OCR – mean OCR following oligomycin injection)], FCCP-induced maximum respiration [mean maximum OCR measurement – final NaN₃ OCR measurement], spare capacity [difference between maximum respiration and (basal respiration - non-mitochondrial respiration)], proton leak [defined as difference between basal respiration and oligomycin-induced ATP-linked respiration], and non-mitochondrial respiration [defined as final plateaued NaN₃ OCR].

Antioxidant exposure

Antioxidant N-acetyl-L-cysteine (NAC) (Sigma-Aldrich, St. Louis, MO) was applied to block production of ROS and alleviate increased IAV viral titers by SWCNTs. Prior to performing experiments, we performed several optimization experiments to ensure that the NAC remained stable and did not drastically alter the pH of the cell culture. We also ensured that no cytotoxicity was observed. In brief, NAC powder was stored at 4 °C until use and the stock was made fresh every time before use in buffered media (pH=7.4). A dose response was performed at 0.5, 1, 5, 10 mM, and it was determined that 5 and 10 mM significantly caused some cell death and also changed the pH significantly. Based on these studies we determined that 1 mM maintained stable pH and did not cause cytotoxicity. We utilized this dose in our studies. Similar to exposure scenarios of SWCNTs and IAV above, SAEC were exposed to SWCNTs for 24 h, then incubated with 1 mM NAC for 2 h, and finally infected with IAV. At the end of the exposure, virus titer, RNA gene expression, ROS production, MMP impairment, and immunofluorescence were measured as described earlier.

Statistics

For most experiments a One-way ANOVA was used to analyze differences between the means. Pair-wise comparisons were conducted by using Tukey's test for equal variances and Dunnett's test for unequal variances. Data were tested for normal distribution for one-way ANOVA and t-test. Data with non-normal distribution would be Log_{10} transformed to achieve normal distribution; if not, data were compared by using Kruskal-Wallis rank-sum test and Dunn's multiple comparison test. Statistical differences were identified at $P < 0.05$.

Results

Materials characterization and cytotoxicity of SWCNTs

Since the characteristics and behavior of nanomaterials has been shown to differ from prepared working stocks, we determined several physicochemical properties of SWCNTs in cell culture media. The dynamic light scattering (DLS) and electrophoretic mobility (EPM) measurements were used to discern size and surface potential. We also determined leaching of metal components into the advanced Roswell Park Memorial Institute (RPMI) 1640 media after a final concentration of 10 $\mu\text{g}/\text{mL}$ SWCNTs were incubated in the media for 24 h. Our working stocks were prepared by suspending SWCNTs (SG65) in 1% pluronic solution prior to adding to the cell media (Sanpui et al., 2014; Bisesi et al., 2015). The average hydrodynamic radius (HDR) of SWCNTs in RPMI media was 280.1 ± 201.5 nm (Fig. 1A, Suppl. Fig. 1). The zeta potential, determined from the EPM, was -2.4 ± 0.6 mV (EPM of $-0.2 \pm 0.1 \times 10^{-8} \text{m}^2 \text{V}^{-1} \text{s}^{-1}$) (Fig. 1A). Trace metal analysis of cell culture media containing SWCNTs was compared to media only after a 24 h incubation period. Molybdenum (Mo, 35ppm), selenium (Se, 28 ppm), silicon (Si, 300 ppm), and zinc (Zn, 240 ppm) showed higher levels in the SWCNT-containing group compared to control media (Suppl. Tab. 1).

To determine the cytotoxicity of SWCNTs, we performed a trypan blue assay (due to interference with MTT assay) in SAEC exposed to a range of doses (0.2 to 50 $\mu\text{g}/\text{mL}$ or 0.5 to 13.2 $\mu\text{g}/\text{cm}^2$) of SWCNTs for 24 h. Results of these experiments show that cell viability

was significantly reduced only at the higher doses tested (20 and 50 $\mu\text{g}/\text{mL}$), compared to that of the control cells. It is important to note that the decrease in cell viability, while significant, was minimal, averaging $\sim 6\%$ reduction (Fig. 1B).

Time-dependent expression of antiviral defense genes in SAEC

To establish a baseline data of immune defense responses of SAEC to IAV infection, cells were exposed to IAV (Influenza virus H1N1 strain A/Mexico/4108/2009) for 2, 4, 8, 12, 18, and 24 h, and the mRNA expression of several antiviral and pro-inflammatory genes was quantified. Results show that the expression of influenza matrix protein 2 (*M2*) RNA is highly induced with peak levels occurring 18 h post-infection. Viral RNA sensors within host cells including Toll-like receptor 3 (*TLR3*), *RIG-I*, and *MDA5* were all highly and significantly induced beginning at 8–12 h post-infection, and these levels of expression were maintained and, in some cases, increased throughout the 24 h period. (Fig. 2)

We also examined changes in expression of several downstream adapters known to control innate immune signaling pathways that are driven by activated TLRs and RIG-I. The TLR2/7 adaptor, myeloid differentiation primary response 88 protein gene (*MyD88*) was induced approximately 2-fold by IAV compared with control cells for most time-points, whereas the mRNA levels for RIG-I/MDA5 adaptor, *MAVS*, and its regulator nucleotide-binding oligomerization domain, leucine rich repeat containing X1 (*NLRX1*) were not significantly altered compared to control cells at any of the time-points. (Fig. 2)

Downstream antiviral transcriptional targets of PRR pathways including interferon beta 1 (*IFN β 1*), *IFIT2*, *IFIT3*, and C-C Motif Chemokine Ligand 5 (*CCL5*) were significantly induced starting at 4–8 h post-infection. However, the mRNA levels of interleukin 8 (*IL-8*) showed a unique expression pattern with significantly increased levels measured as early as 2 h post-infection compared to control. Levels peaked at 4 h and continued to decrease throughout the rest of the time-course, reaching control levels by 24 h post-infection. (Fig. 2)

It should be noted that the baseline levels of each gene (compared to the entire set of gene targets) differed and these data are presented in Suppl. Fig. 2. Genes are listed from left to right in order of the lowest expression level (for control 2h samples) to the highest levels (i.e. *CCL5* to *MyD88*). This highlights that most of the genes impacted least by IAV, are those that are ‘constitutive’ and most highly expressed normally (i.e. *NLRX1*, *MAVS*, *MyD88*).

SWCNTs inhibit IAV-induced antiviral and pro-inflammatory genes and titers through the RLR pathway

With solid baseline data showing the change in expression of immune genes in response to IAV infection, we then determined whether SWCNTs would alter this typical response. To investigate this notion, we exposed cells to various doses of SWCNTs (0.2, 2.0, 20.0, and 50.0 $\mu\text{g}/\text{mL}$) for 24 h, followed by exposure to IAV for an additional 24 h and quantified mRNA levels of several antiviral and pro-inflammatory genes (*TLR3*, *RIG-I*, *MDA5*, *MAVS*, *NLRX1*, *MyD88*, *IFN β 1*, *IFIT2*, *IFIT3*, *CCL5*, *IL-8*, and surfactant protein D (*SPFD*)). Several notable observations are apparent from these data: exposure to SWCNTs

alone did not significantly alter the mRNA levels of most of the genes tested, except for increased expression of *MyD88* by the highest dose of SWCNTs; exposure to IAV alone significantly induced the expression of *TLR3*, *RIG-I*, *MDA5*, *IFN β 1*, *IFIT2*, *IFIT3*, *CCL5*, and *slightly IL-8*, but not *MAVS*, *NLRX1*, *MyD88*, or *SFPD*, consistent with the previous 24 h time course experiment described above; exposure of SAEC to SWCNTs followed by IAV infection showed significant inhibition of the mRNA levels for several IAV-induced genes with a dose-dependent trend (*TLR3*, *RIG-I*, *MDA5*, *IFN β 1*, *IFIT2*, *IFIT3*, *CCL5*), but not of *IL-8* (Fig. 3).

To discern the consequences of inhibition of anti-viral defenses in viral infection, SAEC were exposed to several doses of SWCNTs for 24-h followed by IAV (MOI=0.5) exposure for another 24 h and viral titers and mRNA expression of the *M2* gene were conducted. Results from these studies show that, compared with IAV only exposed cells, pre-exposure of SWCNTs significantly increased the IAV titers, reaching a 3.4-fold increase at the highest dose tested (Tab. 1). Interestingly, mRNA levels of IAV *M2* showed an inverse trend at all doses of SWCNTs tested compared to viral titers (Tab. 1).

Production of reactive oxidative species by SWCNTs and IAV

We tested if SWCNTs and IAV singly or together could produce ROS in SAEC. Results of these experiments show that SWCNT exposure alone induced reactive oxygen species (ROS) production in a dose-dependent manner with significant changes occurring at 20 and 50 $\mu\text{g}/\text{mL}$ at 4 hours post-exposure (Fig. 4A). These levels were also observed after 2, 4 and 6 hours of SWCNT exposure (Suppl. Fig. 3) with levels reaching a plateau that was maintained up to 24 hours (Suppl. Fig. 4A). However, IAV exposure alone failed to significantly increase ROS production at any doses tested (4 hours post infection), although at the highest dose (MOI=5.0), there is an increasing trend (Fig. 4B). It is important to note that our exposures described above were performed using doses IAV (MOI =0.5) that produced no ROS. Since the ROS dye (DCFDA) is not stable beyond 6 hours, we designed a co-exposure scenario that allowed us to determine if the presence of SWCNTs would lead to enhanced ROS production with the virus at varied time-points post infection. Exposure to SWCNTs (50 $\mu\text{g}/\text{mL}$) followed by IAV infection (MOI =0.5) of SAEC led to a slightly increased production of ROS compared with that of SWCNT treatment alone (2 fold vs. 3 fold), but ROS production among SWCNT+IAV groups was not statistically different at any time-points (Fig. 4C). This notion was further tested with varied doses of virus which showed the same results (Suppl. Fig. 4B). The antioxidant NAC was used to mitigate production of ROS in SAEC by SWCNTs. Exposure of SAEC to NAC completely blocked ROS production by SWCNTs alone. However, in the presence of SWCNTs and IAV, NAC treatment only partially reduced ROS production, independent of time-points (Fig. 4C).

We also measured mRNA levels of several genes that reflect a typical cellular response to oxidative stress which included superoxide dismutase 2 (*SOD2*), glutathione peroxidase 1 (*GPX1*), and heme oxygenase 1 (*HMOX1*). As expected, SWCNTs alone led to a significant increase in *SOD2*, *GPX1*, and *HMOX1* expression at the highest dose (50 $\mu\text{g}/\text{mL}$), while IAV alone or together with any doses of SWCNTs did not significantly change the expression levels of any of these targets (Fig. 5).

SWCNTs alter mitochondrial membrane potential

Mitochondrial membrane potential (MMP) and related parameters were measured in cells which were exposed to different doses of SWCNTs, IAV or the combination (SWCNTs + IAV) as described above. Results show that 20 and 50 $\mu\text{g}/\text{mL}$ SWCNTs decreased MMP (Fig. 6A). This decrease was also accompanied by increased mRNA levels of mitofusin 1 and 2 (*MFN1*, *MFN2*) (Fig. 6D, E). Surprisingly, despite changes in MMP, mitochondrial bioenergetics of SAEC, which included basal respiration, oligomycin-induced ATP production, FCCP-induced maximum respiration, spare respiratory capacity, proton leak, and non-mitochondrial respiration were not significantly altered by SWCNTs compared to control cells (Fig. 7). This finding was also supported by an initial metabolomics experiment in which metabolites used for mitochondrial energy production (citric acid cycle) were measured by Nuclear Magnetic Resonance (NMR); no metabolite quantified was significantly altered in abundance by SWCNTs (Supp. Tab. 3.). Compared to SWCNTs, IAV alone did not significantly alter MMP or changes in expression of *MFN1* or *MFN2* from controls at any of the doses tested (Fig. 6B, D, and E). Surprisingly, exposure to SWCNTs followed by IAV (MOI=0.5) significantly increased MMP at SWCNT doses of 0.2, 2.0, and 20.0 $\mu\text{g}/\text{mL}$ (Fig. 6C).

SWCNTs inhibit RLR/MAVS signaling in SAEC

We used immunofluorescence to investigate whether SWCNTs could impair MAVS aggregate formation at the protein level. Figure 8 shows that MAVS (green) is well-dispersed in the cytoplasmic area around the nucleus (blue) and is associated with the mitochondria (red) in the unexposed control cells. However, after IAV exposure, the distribution of MAVS becomes localized, primarily on one side of the cell and displays as an aggregate. Cells that were exposed to SWCNTs (50 $\mu\text{g}/\text{mL}$) followed by IAV infection showed a mixed profile of MAVS distribution. Some cells showed dispersed MAVS similar to control cells, whereas other cells in the same population seemed to form aggregates similar to IAV infected cells (Fig. 8).

SWCNTs increased viral titers and inhibited antiviral gene expression via ROS production

Antioxidant was applied to investigate if blocking ROS would alleviate the increased viral titer and restore inhibited innate immune pathway by SWCNTs. As shown in Figure 9, SWCNTs significantly increased IAV virus titers of SAEC with dose-dependent increases reaching approximately 4 to 5.6 fold by SWCNTs at 20.0 and 50.0 $\mu\text{g}/\text{mL}$, respectively. With NAC treatment, increased viral titers by SWCNTs were significantly reduced to approximately a 2-fold change from the control. There are more MAVS aggregated cells in NAC pre-treated cells following SWCNTs + IAV exposure than those in SWCNTs + IAV treatment (Fig. 8). Consequences of MAVS-declustering was measured at the gene expression level. As expected, SWCNTs significantly decreased the IAV-induced mRNA levels of *RIG-I*, *MDA5*, *IFN β 1*, *IFIT2*, *IFIT3*, and *CCL5*. NAC treatment significantly altered this response for several targets, whereby the repression observed by SWCNTs was not as robust (Fig. 10). For example, there was no significant reduction of IAV-induced *RIG-I* by SWCNTs (Fig. 10), when ROS production was blocked by NAC. Similar results were

observed for *IFN β 1* and *CCL5*, whereas partial rescue of gene expression was evident for *MDA5* and *IFITs*.

Discussion

We report here for the first time that exposure to SWCNTs can modulate innate immune pathways, specifically RLR/MAVS, and increase viral titers to IAV through oxidative stress. Current findings of increased susceptibility to infectious agents induced by NMs are consistent with our previous work and align well with other similar studies (Chen et al., 2017; Kisin et al., 2011; Sanpui et al., 2014; Sattler et al., 2017; Shvedova et al., 2008). The doses used here fall within the reported occupational exposure range of 1 to 70 $\mu\text{g}/\text{m}^3$ (Dahm et al., 2018; Kouassi et al., 2017) and are consistent with (and in many cases lower than) other *in vitro* assessment studies for CNTs (Clift et al., 2014; Mrakovcic et al., 2015; Park et al., 2014). We observed higher concentrations of several metals (e.g. Mo, Zn, Se) in the SWCNT media as expected (e.g. Mo is a known catalyst used in the synthesis of SWCNTs) (Duque et al., 2009). However, the levels detected were well below those associated with reported toxicity in humans (Liu et al., 2013).

The model virus was a wild-type, low-passage strain of influenza virus that belongs to the genetic lineage of IAV responsible for the pandemic that occurred in 2009, and is known to induce robust immune responses that include interferons, IFITs, IL-8, and CCL5 (Duffney et al., 2018; Jorgensen et al., 2018; Rowe et al., 2010). Our findings are consistent with the literature, which shows that *IFIT2*, *IFIT3*, *IFN β 1*, and *CCL5* are significantly induced prior to 24 h post-infection to IAV in lung epithelial cells (Chan et al., 2010; Varga et al., 2012). The M2 is a multifunctional viral transmembrane protein that plays critical roles in controlling viral entry, replication, and egress (Pielak & Chou, 2011), and the expression of M2 RNA was quantified as a measure of viral infection. The high levels of M2 mRNA were also associated with the increased mRNA levels of several gene targets that sense viral RNA molecules within cells and include *TLR3*, *RIG-I*, and *MDA5*. The relatively unchanged expression of RLR adaptor *MAVS* and its regulator *NLRX1* is not unusual as several reports show these proteins to be highly and constitutively expressed, and are therefore 'ready' to promote signaling quickly when viral molecules are sensed by TLRs and RIG-I/MDA5 (Jacobs et al., 2014; Koshiba et al., 2011). The fact that *IL-8* levels peaked earlier than other targets is also in agreement with a reported biphasic response of cytokines/chemokines in response to viral infections in bronchial epithelial cells (BEAS-2B), and it is also likely explained by known regulation through other pathways, such as TGF- α /EGFR signaling (Griego et al., 2000; Ito et al., 2015).

Consistent with our previous studies (Chen et al., 2017; Sanpui et al., 2014), SWCNTs alone did not significantly alter the mRNA levels of most of the antiviral and pro-inflammatory genes tested, except *MyD88* at the highest dose (50 $\mu\text{g}/\text{ml}$). MyD88 serves as an adaptor protein to several toll-like receptors (i.e. TLR2, TLR4, TLR7) and interleukin-1 receptors (IL-1R) (Turabekova et al., 2014; Meng et al., 2015). Since *TLR3* and *IFN β 1* are reduced (at least at the mRNA level), the increase in *MyD88* could be a compensatory response in efforts to activate these receptors.

SWCNTs were also able to inhibit the expression of antiviral and pro-inflammatory genes such as *IFN β 1*, *IFIT2*, *IFIT3*, and *CCL5* as well as their upstream viral RNA sensors including *TLR3*, *RIG-I*, and *MDA5*, but not *IL-8*. This uninhibited *IL-8* expression by SWCNTs was also recently noted in lung cells in response to silver nanoparticles where *CCL-5* was repressed, yet *IL-8* levels were induced (Villeret et al., 2018). Other environmental chemicals/pollutants, such as cigarette smoke, have been shown to modulate innate immune responses to influenza infections by inhibiting antiviral mediators (e.g. interferons and *IP-10*) and *IL-8* through impairment of *TLR3* activation at both mRNA and protein levels (Duffney et al., 2018). The increased viral titer with exposure to SWCNTs demonstrates that impairment of viral defense systems leads to cells that are more susceptible to viral infection. However, it's surprising that the mRNA expression of *M2* was not correspondingly increased with viral titer. The measure of *M2* expression is an indication of how much viral genetic material is made but does not necessarily tell us anything about other aspects of the viral life cycle, such as turnover of genetic material and formation and/or release of viral progeny. It should also be noted that we only present data for one time-point which could play a role in the inverse patterns observed for the *M2* expression and titer data. For example, one study showed that alterations in cytokine production was associated with enhance viral particle egress (Ebola virus) (Okumura et al., 2015).

It has been hypothesized that oxidative stress initiated via the production of (ROS) is a primary mechanism of CNT toxicity (Dong & Ma, 2015; Shvedova et al, 2012). However, no studies to-date have assessed ROS production caused by SWCNTs in the context of a respiratory virus, specifically IAV, and the ability of such a trigger to modulate RLR signaling. The production of ROS typically leads to induction of antioxidant genes that are essential for protection from oxidative stress such as *SOD2* which can catalyze extracellular dismutation of O_2^- to H_2O_2 , while *GPX1* processes H_2O_2 into water and oxygen (Levonen et al., 2008). *HMOX1* is also known to be induced by oxidative stress and plays a protective role in oxidative damage (Levonen et al., 2008). The significantly induced *SOD2*, *GPX1*, and *HMOX1* expression are consistent with the notion of enhanced ROS production in SAEC by SWCNTs and a lack of ROS production by IAV.

Our results however, are in contrast to other reports that demonstrate IAV exposure at MOI=0.01 caused significant increases of superoxide anion and H_2O_2 in A549 cells at 24-h post-infection while inhibiting *SOD* expression (Pyo et al., 2014). Other strains of IAV, including H9N2 and different subtypes of H3N2, have also been shown to increase *HMOX1*, *GPX1* and *SFPD* expression in both cells and mice, suggesting that these genes display protective roles in IAV infection, inflammation, and cellular damage (Cummins et al., 2012; LeVine et al., 2001; Qi et al., 2018; Yatmaz et al., 2013). It is possible that the discrepancy of IAV-induced expression of these oxidative stress genes between studies is a result of the experimental models used (*in vivo* vs. *in vitro*, different cell lines, sensitive time-points, etc.).

The mitochondria serve to regulate several cellular functions in response to stress that include respiration and energy production, immune responses, and cell death (i.e. apoptosis). Mitochondria rely on several parameters for normal function such as MMP, which is

generated by redox transformations associated with the activity of the Citric Acid cycle and is crucial for cellular ATP production (Zorov et al., 2014; Zorova et al., 2017). Similar to our results, some studies showed SWCNTs can significantly reduce MMP as early as 1 h after exposure and can decrease MMP by about 70% after 48 h (Naserzadeh et al., 2018; Zeinabad et al., 2016). Dissipation of MMP typically inhibits mitochondrial fusion leading to mitochondrial fragmentation, while re-establishment of MMP requires filament network reconstruction (Ishihara et al., 2004). Both MFN1 and MFN2 mediate mitochondrial tethering and function in the mitochondrial fusion process (Ishihara et al., 2004), thus increased MFN1 and MFN2 in response to decreased MMP were anticipated and observed in our results.

While there are not an abundance of studies that have assessed the impact of IAV on MMP, a few reports show that IAV H5N1 protein PB1-F2 interacts directly with MAVS, which leads to lowered MMP and ultimately reduced interferon levels (Varga et al., 2012). Our results are not consistent with this model; however, this may be due to variable timing, virus strain and cell type (Koshiba et al., 2011). Interestingly, MMP were first peaked and decreased when SAEC were exposed to different doses of SWCNTs and IAV. Increased MMP or mitochondrial hyperpolarization (MHP) has been reported in the literature in several cell types in response to chemically-generated oxidative stress (Buskiewicz et al., 2016). The functional role that MHP plays in response to stress is not clear but has been hypothesized to serve as an early, yet transient event, that precedes caspase activation that eventually leads to apoptosis (Giovannini et al., 2002; Matarrese et al., 2003; Nagy et al., 2007). Under our specific exposure scenario, cells first undergo depolarization by SWCNTs, but then move to a state of hyperpolarization after the addition of virus. This significant 'switch' has not to our knowledge been reported in the literature in response to the combined stress of nanoparticles and pathogens.

The unaffected mitochondrial oxygen consumption rate (OCR) indicates there may be a strong compensatory mechanism by which SAEC can overcome impaired MMP observed in response to SWCNTs. Changes in MMP, such as the decrease in response to SWCNT exposure, may trigger autophagy, a process which promotes energy efficiency through ATP production and mediates damage control by removing non-functional proteins and organelles in response to stress (Glick et al., 2010). Since the data discussed above support repression, at least in part, of RLR signaling by SWCNTs and modulation of mitochondrial parameters, we designed a set of experiments to probe functional aspects of this pathway that rely on the mitochondria. It has been recently documented that activation of RIG-I/MAVS signaling is dependent on prion-like aggregate formation of MAVS protein located on the mitochondria, which then 'docks' with the RIG-I-MAVS complex to form the MAVS signalosome (Hou et al., 2011). This process occurs once viruses are sensed by RIG-I/MDA5. The aggregates of MAVS formation after IAV exposure in our study is consistent with the literature and the pattern of MAVS localization when activated by viruses (Jacobs et al., 2014; Koshiba et al., 2011; Varga et al., 2012). When docking occurs, signaling continues to initiate the production of anti-viral responses that include production of interferons, IFITs, and other chemokines/cytokines. Interestingly, exposure to SWCNTs + IAV reduced the cell population presenting features of MAVS aggregation. These observations suggest that there is a partial impairment of MAVS aggregation, which could

contribute to the overall repression of the immune response as measured by decreased gene expression. Partial impairment may also be a result of a heterogeneously impacted cell population. Based on our data, we cannot discern which cells exactly are infected or have direct interaction with the nanotubes. What we can postulate is that at the viral dose (MOI=0.5) we expect half of the cells initially (0.5 particles per cell) would be infected, but this dose is high enough that neighboring cells would also become infected by produced progeny. We are also giving a dose of nanotubes that we expect would impact the majority of cells. However, at any given time there may be some heterogeneity in the cell population with respect to whether each individual cell is impacted by both agents and this notion required further investigation.

If the over-production of ROS is a driver for SWCNT-induced repression of innate immunity and subsequent increased viral titer after IAV infection, then blocking ROS or alleviating oxidative stress would lead to a loss of the effects caused by SWCNTs. Our experiments have shown that NAC can block ROS production induced by SWCNTs in SAEC which was consistent with findings from similar studies (Avalos et al., 2014; Hou et al., 2016; Kim & Yu, 2014). NAC acts as a precursor for the substrate cysteine in the synthesis of glutathione and also as a mucolytic and anti-inflammatory agent (Geiler et al., 2010; Matera et al., 2016). Besides increased IAV titer by SWCNTs was reduced by NAC, the SWCNT-inhibition of IAV-induced MAVS clustering and its downstream immune responses was also partially restored by NAC. These results indicate that ROS production is a major contributor to the mechanisms by which SWCNTs enhance IAV infection.

It should also be noted that data from our ROS assays indicate that IAV alone does not produce significant ROS. While we were surprised by this result, the production of ROS is strain specific, as is the ability of NAC to block viral replication (Garigliany & Desmecht, 2011). Several reports demonstrate the effect of NAC on virus replication and expression of pro-inflammatory molecules. One study showed that cells exposed to NAC prior to H5N1 infection resulted in decreased viral replication and expression of pro-inflammatory markers (Geiler et al., 2010). NAC was also shown to reduce pulmonary inflammation caused by exposure to diesel exhaust and influenza to levels induced only by the virus alone in mice, although this study did not observe decreased viral titers with NAC (Gowdy et al., 2010). Though interaction of ROS and RLR signaling pathway was notable in our results, we cannot rule out contribution from other PRR pathways (i.e. TLRs, NLRs), which would require extensive investigations (i.e. siRNA) to address this more specifically. Regardless, our data point to RLR as a target of SWCNT-induced dysfunction, in this case, enhanced susceptibility to IAV infection through ROS production.

Few studies have investigated the ability of nanomaterials to alter innate immune pathways that control host defenses to viral infections. In a recent study, Villeret and colleagues elegantly showed that silver- but not gold-nanoparticles impaired viral-induced RLR signaling, as evidenced by repression of *CCL-5* expression, autophagy, and IRF7 activity (Villeret et al., 2018). They further showed that the generation of silver ions contributed partially to these observed effects. Our results show the ability of yet another nanoparticle of distinct composition (carbon and with minimum ionic release) to also target the RLR signaling pathway. In addition, and for the first time, we reveal repression of selected anti-

viral gene expression (IFITs) and impairment of MAVS aggregate formation that is dependent, partially, on oxidative stress production with no apparent impairment of mitochondrial respiratory capacity. While the former study showed no effects on viral replication, our data support the idea that the viral packaging and egress may be more effective as levels of M2 were reduced in the presence of SWCNTs, yet viral titers significantly increased. We also note a more robust rescue of effects when the antioxidant NAC was employed. Overall, this study suggests that select nanoparticles of varied type can impair innate host defense systems that are essential in mitigating viral infections.

Conclusions

Pulmonary exposure to SWCNTs not only induces robust inflammation, fibrosis, granuloma formation, and pre-cancerous lesions (Beard et al., 2018; Cesta et al., 2010; Donaldson et al., 2013; Dong & Ma, 2016; Dong et al., 2015; Shvedova et al., 2005), but may also render hosts more susceptible to respiratory infections by pathogens such as influenza virus (Chen et al., 2017; Sanpui et al., 2014) by repressing immune defense responses. Results of the present study show for the first time that pristine SWCNTs inhibit innate immune responses to IAV infection, at least partially, through oxidative stress production and mitochondrial damage (Fig. 11). Of particular note is the impairment of MAVS aggregation on the mitochondria, which is known to impair RLR signaling and consequently transcription of anti-viral genes that include IFITs and interferons. Without these defenses, we speculate that IAV can replicate more efficiently, leading to significantly higher titers in the presence of SWCNTs. Future studies should investigate the role of SWCNT-induced ROS production and impairment of RLR signaling translates to in *in vivo* models and the impact of other types of CNTs (e.g. MWCNT) on IAV susceptibility

Supplementary Material

Refer to Web version on PubMed Central for supplementary material.

Acknowledgements

Funding

This work was funded by the National Institute of Health (R01HL114907 to TSA) and R01-DK105346 and U24-DK097209 (to MEM). A portion of this work was performed at the National High Magnetic Field Laboratory, which is supported by National Science Foundation Cooperative Agreement No. DMR-1644779 and the State of Florida. The funders had no role in study design, data collection and analysis, decision to publish, or preparation of the manuscript.

REFERENCES

- Afroz AR, Khan IA, Hussain SM, & Saleh NB (2013) (a) Mechanistic heteroaggregation of gold nanoparticles in a wide range of solution chemistry. *Environ Sci Technol*, 47(4), 1853–1860. doi: 10.1021/es3032709 [PubMed: 23360522]
- Afroz ARMN, Khan IA, Hussain SM, & Saleh NB (2013) (b) Mechanistic Heteroaggregation of Gold Nanoparticles in a Wide Range of Solution Chemistry. *Environ Sci Technol*, 47(4), 1853–1860. doi: Doi 10.1021/Es3032709 [PubMed: 23360522]

- Aich N, Boateng LK, Sabaraya IV, Das D, Flora JR, & Saleh NB (2016). Aggregation Kinetics of Higher-Order Fullerene Clusters in Aquatic Systems. *Environ Sci Technol*, 50(7), 3562–3571. doi: 10.1021/acs.est.5b05447 [PubMed: 26928084]
- Avalos A, Haza AI, Mateo D, & Morales P (2014). Cytotoxicity and ROS production of manufactured silver nanoparticles of different sizes in hepatoma and leukemia cells. *J Appl Toxicol*, 34(4), 413–423. doi: 10.1002/jat.2957 [PubMed: 24243578]
- Beard JD, Erdely A, Dahm MM, de Perio MA, Birch ME, Evans DE, Schubauer-Berigan MK (2018). Carbon nanotube and nanofiber exposure and sputum and blood biomarkers of early effect among U.S. workers. *Environment International*, 116, 214–228. doi: 10.1016/j.envint.2018.04.004 [PubMed: 29698898]
- Bisesi JH, Ngo T, Ponnayolu S, Liu K, Lavelle CM, Afrooz AR, Sabo-Attwood T (2015). Examination of Single-Walled Carbon Nanotubes Uptake and Toxicity from Dietary Exposure: Tracking Movement and Impacts in the Gastrointestinal System. *Nanomaterials (Basel)*, 5(2), 1066–1086. doi: 10.3390/nano5021066 [PubMed: 28347052]
- Buskiewicz IA, Montgomery T, Yasewicz EC, Huber SA, Murphy MP, Hartley RC, Koenig A (2016). Reactive oxygen species induce virus-independent MAVS oligomerization in systemic lupus erythematosus. *Sci Signal*, 9(456), ra115. doi: 10.1126/scisignal.aaf1933 [PubMed: 27899525]
- Cesta MF, Ryman-Rasmussen JP, Wallace DG, Masinde T, Hurlburt G, Taylor AJ, & Bonner JC (2010). Bacterial lipopolysaccharide enhances PDGF signaling and pulmonary fibrosis in rats exposed to carbon nanotubes. *Am J Respir Cell Mol Biol*, 43(2), 142–151. doi: 10.1165/rcmb.2009-0113OC [PubMed: 19738159]
- Chan MC, Chan RW, Yu WC, Ho CC, Yuen KM, Fong JH, Peiris JS (2010). Tropism and innate host responses of the 2009 pandemic H1N1 influenza virus in ex vivo and in vitro cultures of human conjunctiva and respiratory tract. *Am J Pathol*, 176(4), 1828–1840. doi: 10.2353/ajpath.2010.091087 [PubMed: 20110407]
- Chen H, Zheng X, Nicholas J, Humes ST, Loeb JC, Robinson SE, Sabo-Attwood T (2017). Single-walled carbon nanotubes modulate pulmonary immune responses and increase pandemic influenza a virus titers in mice. *Virology*, 14(1), 242. doi: 10.1186/s12985-017-0909-z [PubMed: 29273069]
- Clift MJ, Endes C, Vanhecke D, Wick P, Gehr P, Schins RP, Rothen-Rutishauser B (2014). A comparative study of different in vitro lung cell culture systems to assess the most beneficial tool for screening the potential adverse effects of carbon nanotubes. *Toxicol Sci*, 137(1), 55–64. doi: 10.1093/toxsci/kft216 [PubMed: 24284789]
- Cummins NW, Weaver EA, May SM, Croatt AJ, Foreman O, Kennedy RB, Badley AD (2012). Heme oxygenase-1 regulates the immune response to influenza virus infection and vaccination in aged mice. *FASEB J*, 26(7), 2911–2918. doi: 10.1096/fj.11-190017 [PubMed: 22490782]
- Dahm MM, Schubauer-Berigan MK, Evans DE, Birch ME, Bertke S, Beard JD, Grinshpun SA (2018). Exposure assessments for a cross-sectional epidemiologic study of US carbon nanotube and nanofiber workers. *Int J Hyg Environ Health*, 221(3), 429–440. doi: 10.1016/j.ijheh.2018.01.006 [PubMed: 29339022]
- Donaldson K, Poland CA, Murphy FA, MacFarlane M, Chernova T, & Schinwald A (2013). Pulmonary toxicity of carbon nanotubes and asbestos - similarities and differences. *Adv Drug Deliv Rev*, 65(15), 2078–2086. doi: 10.1016/j.addr.2013.07.014 [PubMed: 23899865]
- Dong J, & Ma Q (2015). Advances in mechanisms and signaling pathways of carbon nanotube toxicity. *Nanotoxicology*, 9(5), 658–676. doi: 10.3109/17435390.2015.1009187 [PubMed: 25676622]
- Dong J, & Ma Q (2016). Suppression of basal and carbon nanotube-induced oxidative stress, inflammation and fibrosis in mouse lungs by Nrf2. *Nanotoxicology*, 10(6), 699–709. doi: 10.3109/17435390.2015.1110758 [PubMed: 26592091]
- Dong J, Porter DW, Batteli LA, Wolfarth MG, Richardson DL, & Ma Q (2015). Pathologic and molecular profiling of rapid-onset fibrosis and inflammation induced by multi-walled carbon nanotubes. *Archives of toxicology*, 89(4), 621–633. [PubMed: 25510677]
- Duffney PF, McCarthy CE, Nogales A, Thatcher TH, Martinez-Sobrido L, Phipps RP, & Sime PJ (2018). Cigarette smoke dampens antiviral signaling in small airway epithelial cells by disrupting TLR3 cleavage. *Am J Physiol Lung Cell Mol Physiol*, 314(3), L505–L513. doi: 10.1152/ajplung.00406.2017 [PubMed: 29351447]

- Duque JG, Pasquali M, Cognet L, & Lounis B (2009). Environmental and synthesis-dependent luminescence properties of individual single-walled carbon nanotubes. *ACS Nano*, 3(8), 2153–2156. doi: 10.1021/nn9003956 [PubMed: 19594113]
- Garigliany MM, & Desmecht DJ (2011). N-acetylcysteine lacks universal inhibitory activity against influenza A viruses. *J Negat Results Biomed*, 10, 5. doi: 10.1186/1477-5751-10-5 [PubMed: 21554703]
- Geiler J, Michaelis M, Naczek P, Leutz A, Langer K, Doerr HW, & Cinatl J Jr. (2010). N-acetyl-L-cysteine (NAC) inhibits virus replication and expression of pro-inflammatory molecules in A549 cells infected with highly pathogenic H5N1 influenza A virus. *Biochem Pharmacol*, 79(3), 413–420. doi: 10.1016/j.bcp.2009.08.025 [PubMed: 19732754]
- Giovannini C, Matarrese P, Scazzocchio B, Sanchez M, Masella R, & Malorni W (2002). Mitochondria hyperpolarization is an early event in oxidized low-density lipoprotein-induced apoptosis in Caco-2 intestinal cells. *FEBS Lett*, 523(1–3), 200–206. [PubMed: 12123832]
- Glick D, Barth S, & Macleod KF (2010). Autophagy: cellular and molecular mechanisms. *J Pathol*, 221(1), 3–12. doi: 10.1002/path.2697 [PubMed: 20225336]
- Goff PH, Hayashi T, He W, Yao S, Cottam HB, Tan GS, Corr M (2017). Synthetic Toll-Like Receptor 4 (TLR4) and TLR7 Ligands Work Additively via MyD88 To Induce Protective Antiviral Immunity in Mice. *J Virol*, 91(19). doi: 10.1128/JVI.01050-17
- Gowdy KM, Krantz QT, King C, Boykin E, Jaspers I, Linak WP, & Gilmour MI (2010). Role of oxidative stress on diesel-enhanced influenza infection in mice. *Part Fibre Toxicol*, 7, 34. doi: 10.1186/1743-8977-7-34 [PubMed: 21092162]
- Grand View Research, GRV. (2015). Global Carbon Nanotubes (CNT) Market By Product (Single Walled Carbon Nanotubes (SWCNT), Multi Walled Carbon Nanotubes (MWCNT)), By Application (Polymers, Energy, Electrical & Electronics) Is Expected To Reach USD 3.42 Billion By 2022.
- Griego SD, Weston CB, Adams JL, Tal-Singer R, & Dillon SB (2000). Role of p38 mitogen-activated protein kinase in rhinovirus-induced cytokine production by bronchial epithelial cells. *J Immunol*, 165(9), 5211–5220. [PubMed: 11046054]
- Groopman JD, Johnson D, & Kensler TW (2005). Aflatoxin and hepatitis B virus biomarkers: a paradigm for complex environmental exposures and cancer risk. *Cancer Biomark*, 1(1), 5–14. [PubMed: 17192028]
- Hou F, Sun L, Zheng H, Skaug B, Jiang QX, & Chen ZJ (2011). MAVS forms functional prion-like aggregates to activate and propagate antiviral innate immune response. *Cell*, 146(3), 448–461. doi: 10.1016/j.cell.2011.06.041 [PubMed: 21782231]
- Hou J, Wan B, Yang Y, Ren XM, Guo LH, & Liu JF (2016). Biodegradation of Single-Walled Carbon Nanotubes in Macrophages through Respiratory Burst Modulation. *Int J Mol Sci*, 17(3), 409. doi: 10.3390/ijms17030409 [PubMed: 27011169]
- Ishihara N, Eura Y, & Mihara K (2004). Mitofusin 1 and 2 play distinct roles in mitochondrial fusion reactions via GTPase activity. *J Cell Sci*, 117(Pt 26), 6535–6546. doi: 10.1242/jcs.01565 [PubMed: 15572413]
- Ito Y, Correll K, Zemans RL, Leslie CC, Murphy RC, & Mason RJ (2015). Influenza induces IL-8 and GM-CSF secretion by human alveolar epithelial cells through HGF/c-Met and TGF- α /EGFR signaling. *Am J Physiol Lung Cell Mol Physiol*, 308(11), L1178–L1188. doi: 10.1152/ajplung.00290.2014 [PubMed: 26033355]
- Jacobs JL, Zhu J, Sarkar SN, & Coyne CB (2014). Regulation of mitochondrial antiviral signaling (MAVS) expression and signaling by the mitochondria-associated endoplasmic reticulum membrane (MAM) protein Gp78. *J Biol Chem*, 289(3), 1604–1616. doi: 10.1074/jbc.M113.520254 [PubMed: 24285545]
- Jaspers I, Sheridan PA, Zhang W, Brighton LE, Chason KD, Hua X, & Tilley SL (2009). Exacerbation of allergic inflammation in mice exposed to diesel exhaust particles prior to viral infection. *Part Fibre Toxicol*, 6, 22. doi: 10.1186/1743-8977-6-22 [PubMed: 19682371]
- Jorgensen SE, Christiansen M, Ryo LB, Gad HH, Gjedsted J, Staeheli P, Mogensen TH (2018). Defective RNA sensing by RIG-I in severe influenza virus infection. *Clin Exp Immunol*. doi: 10.1111/cei.13120

- Khan IA, Afrooz AR, Flora JR, Schierz PA, Ferguson PL, Sabo-Attwood T, & Saleh NB (2013). Chirality affects aggregation kinetics of single-walled carbon nanotubes. *Environ Sci Technol*, 47(4), 1844–1852. doi: 10.1021/es3030337 [PubMed: 23343128]
- Kim JS, & Yu IJ (2014). Single-wall carbon nanotubes (SWCNT) induce cytotoxicity and genotoxicity produced by reactive oxygen species (ROS) generation in phytohemagglutinin (PHA)-stimulated male human peripheral blood lymphocytes. *J Toxicol Environ Health A*, 77(19), 1141–1153. doi: 10.1080/15287394.2014.917062 [PubMed: 25119736]
- Kisin ER, Murray AR, Sargent L, Lowry D, Chirila M, Siegrist KJ, Shvedova AA (2011). Genotoxicity of carbon nanofibers: are they potentially more or less dangerous than carbon nanotubes or asbestos? *Toxicol Appl Pharmacol*, 252(1), 1–10. doi: 10.1016/j.taap.2011.02.001 [PubMed: 21310169]
- Koshiba T, Yasukawa K, Yanagi Y, & Kawabata S (2011). Mitochondrial membrane potential is required for MAVS-mediated antiviral signaling. *Sci Signal*, 4(158), ra7. doi: 10.1126/scisignal.2001147 [PubMed: 21285412]
- Kotchey GP, Hasan SA, Kapralov AA, Ha SH, Kim K, Shvedova AA, Star A (2012). A natural vanishing act: the enzyme-catalyzed degradation of carbon nanomaterials. *Acc Chem Res*, 45(10), 1770–1781. doi: 10.1021/ar300106h [PubMed: 22824066]
- Kouassi S, Catto C, Ostiguy C, L'Esperance G, Kroeger J, & Debia M (2017). Exposure Assessment in a Single-Walled Carbon Nanotube Primary Manufacturer. *Ann Work Expo Health*, 61(2), 260–266. doi: 10.1093/annweh/wxw017 [PubMed: 28395348]
- LeVine AM, Whitsett JA, Hartshorn KL, Crouch EC, & Korfhagen TR (2001). Surfactant protein D enhances clearance of influenza A virus from the lung in vivo. *J Immunol*, 167(10), 5868–5873. [PubMed: 11698462]
- Levonen AL, Vahakangas E, Koponen JK, & Yla-Herttuala S (2008). Antioxidant gene therapy for cardiovascular disease: current status and future perspectives. *Circulation*, 117(16), 2142–2150. doi: 10.1161/CIRCULATIONAHA.107.718585 [PubMed: 18427144]
- Liao HY, Chung YT, Lai CH, Wang SL, Chiang HC, Li LA, Liou SH (2014). Six-month follow-up study of health markers of nanomaterials among workers handling engineered nanomaterials. *Nanotoxicology*, 8 Suppl 1, 100–110. doi: 10.3109/17435390.2013.858793
- Liu HL, Zhang YL, Yang N, Zhang YX, Liu XQ, Li CG, Jiang CY (2011). A functionalized single-walled carbon nanotube-induced autophagic cell death in human lung cells through Akt-TSC2-mTOR signaling. *Cell Death Dis*, 2, e159. doi: 10.1038/cddis.2011.27 [PubMed: 21593791]
- Liu Y, Zhao Y, Sun B, & Chen C (2013). Understanding the toxicity of carbon nanotubes. *Acc Chem Res*, 46(3), 702–713. doi: 10.1021/ar300028m [PubMed: 22999420]
- Livak KJ, & Schmittgen TD (2001). Analysis of relative gene expression data using real-time quantitative PCR and the 2⁻(-Delta Delta C(T)) Method. *Methods*, 25(4), 402–408. doi: 10.1006/meth.2001.1262 [PubMed: 11846609]
- Mahajan L, Pandit H, Madan T, Gautam P, Yadav AK, Warke H, Surolia A (2013). Human surfactant protein D alters oxidative stress and HMGA1 expression to induce p53 apoptotic pathway in eosinophil leukemic cell line. *PLoS One*, 8(12), e85046. doi: 10.1371/journal.pone.0085046 [PubMed: 24391984]
- Martin CR, & Kohli P (2003). The emerging field of nanotube biotechnology. *Nat Rev Drug Discov*, 2(1), 29–37. doi: 10.1038/nrd988 [PubMed: 12509757]
- Matarrese P, Gambardella L, Cassone A, Vella S, Cauda R, & Malorni W (2003). Mitochondrial membrane hyperpolarization hijacks activated T lymphocytes toward the apoptotic-prone phenotype: homeostatic mechanisms of HIV protease inhibitors. [Comparative Study]. *J Immunol*, 170(12), 6006–6015. [PubMed: 12794128]
- Matera MG, Calzetta L, & Cazzola M (2016). Oxidation pathway and exacerbations in COPD: the role of NAC. *Expert Rev Respir Med*, 10(1), 89–97. doi: 10.1586/17476348.2016.1121105 [PubMed: 26567752]
- Meng J, Li X, Wang C, Guo H, Liu J, & Xu H (2015). Carbon nanotubes activate macrophages into a M1/M2 mixed status: recruiting naive macrophages and supporting angiogenesis. *ACS Appl Mater Interfaces*, 7(5), 3180–3188. doi: 10.1021/am507649n [PubMed: 25591447]

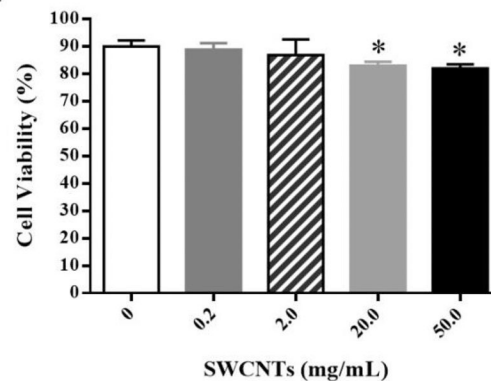
- Mrakovcic M, Meindl C, Leitinger G, Roblegg E, & Frohlich E (2015). Carboxylated short single-walled carbon nanotubes but not plain and multi-walled short carbon nanotubes show in vitro genotoxicity. *Toxicol Sci*, 144(1), 114–127. doi: 10.1093/toxsci/kfu260 [PubMed: 25505129]
- Nagy G, Koncz A, Fernandez D, & Perl A (2007). Nitric oxide, mitochondrial hyperpolarization, and T cell activation. *Free Radic Biol Med*, 42(11), 1625–1631. doi: 10.1016/j.freeradbiomed.2007.02.026 [PubMed: 17462531]
- Naserzadeh P, Ansari Esfeh F, Kaviani M, Ashtari K, Kheirbakhsh R, Salimi A, & Pourahmad J (2018). Single-walled carbon nanotube, multi-walled carbon nanotube and Fe₂O₃ nanoparticles induced mitochondria mediated apoptosis in melanoma cells. *Cutan Ocul Toxicol*, 37(2), 157–166. doi: 10.1080/15569527.2017.1363227 [PubMed: 28768445]
- Okumura A, Rasmussen AL, Halfmann P, Feldmann F, Yoshimura A, Feldmann H, Katze MG (2015). Suppressor of Cytokine Signaling 3 Is an Inducible Host Factor That Regulates Virus Egress during Ebola Virus Infection. *J Virol*, 89(20), 10399–10406. doi: 10.1128/JVI.01736-15 [PubMed: 26246577]
- Park EJ, Hong YS, Lee BS, Yoon C, Jeong U, & Kim Y (2016). Single-walled carbon nanotubes disturbed the immune and metabolic regulation function 13-weeks after a single intratracheal instillation. *Environ Res*, 148, 184–195. doi: 10.1016/j.envres.2016.03.027 [PubMed: 27078092]
- Park EJ, Zahari NE, Lee EW, Song J, Lee JH, Cho MH, & Kim JH (2014). SWCNTs induced autophagic cell death in human bronchial epithelial cells. *Toxicol In Vitro*, 28(3), 442–450. doi: 10.1016/j.tiv.2013.12.012 [PubMed: 24389112]
- Piao CQ, Liu L, Zhao YL, Balajee AS, Suzuki M, & Hei TK (2005). Immortalization of human small airway epithelial cells by ectopic expression of telomerase. *Carcinogenesis*, 26(4), 725–731. doi: 10.1093/carcin/bgi016 [PubMed: 15677631]
- Pielak RM, & Chou JJ (2011). Influenza M2 proton channels. *Biochim Biophys Acta*, 1808(2), 522–529. doi: 10.1016/j.bbamem.2010.04.015 [PubMed: 20451491]
- Pyo CW, Shin N, Jung KI, Choi JH, & Choi SY (2014). Alteration of copper-zinc superoxide dismutase 1 expression by influenza A virus is correlated with virus replication. *Biochem Biophys Res Commun*, 450(1), 711–716. doi: 10.1016/j.bbrc.2014.06.037 [PubMed: 24946209]
- Qi X, Zhang H, Xue T, Yang B, Deng M, & Wang J (2018). Down-regulation of cellular protein heme oxygenase-1 inhibits proliferation of avian influenza virus H9N2 in chicken oviduct epithelial cells. *J Gen Virol*, 99(1), 36–43. doi: 10.1099/jgv.0.000986 [PubMed: 29219807]
- Qian GS, Ross RK, Yu MC, Yuan JM, Gao YT, Henderson BE, Groopman JD (1994). A follow-up study of urinary markers of aflatoxin exposure and liver cancer risk in Shanghai, People's Republic of China. *Cancer Epidemiol Biomarkers Prev*, 3(1), 3–10. [PubMed: 8118382]
- Qin Y, Li S, Zhao G, Fu X, Xie X, Huang Y, Lai Z (2017). Long-term intravenous administration of carboxylated single-walled carbon nanotubes induces persistent accumulation in the lungs and pulmonary fibrosis via the nuclear factor-kappa B pathway. *Int J Nanomedicine*, 12, 263–277. doi: 10.2147/ijn.s123839 [PubMed: 28115845]
- Rowe T, Banner D, Farooqui A, Ng DC, Kelvin AA, Rubino S, Kelvin DJ (2010). In vivo ribavirin activity against severe pandemic H1N1 Influenza A/Mexico/4108/2009. *J Gen Virol*, 91(Pt 12), 2898–2906. doi: 10.1099/vir.0.024323-0 [PubMed: 20797971]
- Sanpui P, Zheng X, Loeb JC, Bisesi JH Jr., Khan IA, Afroz AR, Sabo-Attwood T (2014). Single-walled carbon nanotubes increase pandemic influenza A H1N1 virus infectivity of lung epithelial cells. *Part Fibre Toxicol*, 11, 66. doi: 10.1186/s12989-014-0066-0 [PubMed: 25497303]
- Sattler C, Moritz F, Chen S, Steer B, Kutschke D, Irmeler M, Stoeger T (2017). Nanoparticle exposure reactivates latent herpesvirus and restores a signature of acute infection. *Part Fibre Toxicol*, 14(1), 2. doi: 10.1186/s12989-016-0181-1 [PubMed: 28069010]
- Shvedova AA, Fabisiaik JP, Kisin ER, Murray AR, Roberts JR, Tyurina YY, Kagan VE (2008). Sequential exposure to carbon nanotubes and bacteria enhances pulmonary inflammation and infectivity. *Am J Respir Cell Mol Biol*, 38(5), 579–590. doi: 10.1165/rcmb.2007-0255OC [PubMed: 18096873]
- Shvedova AA, Kisin ER, Mercer R, Murray AR, Johnson VJ, Potapovich AI, Baron P (2005). Unusual inflammatory and fibrogenic pulmonary responses to single-walled carbon nanotubes in mice. *Am*

- J Physiol Lung Cell Mol Physiol, 289(5), L698–708. doi: 10.1152/ajplung.00084.2005 [PubMed: 15951334]
- Shvedova AA, Kisin ER, Porter D, Schulte P, Kagan VE, Fadeel B, & Castranova V (2009). Mechanisms of pulmonary toxicity and medical applications of carbon nanotubes: Two faces of Janus? *Pharmacol Ther*, 121(2), 192–204. doi: S0163–7258(08)00217–9 [pii]10.1016/j.pharmthera.2008.10.009 [PubMed: 19103221]
- Shvedova AA, Pietroiusti A, Fadeel B, & Kagan VE (2012). Mechanisms of carbon nanotube-induced toxicity: focus on oxidative stress. *Toxicol Appl Pharmacol*, 261(2), 121–133. doi: 10.1016/j.taap.2012.03.023 [PubMed: 22513272]
- Sturm R (2014). Clearance of carbon nanotubes in the human respiratory tract—a theoretical approach. *Ann Transl Med*, 2(5), 46. doi: 10.3978/j.issn.2305-5839.2014.04.12 [PubMed: 25333021]
- Sun Y, Li C, Shu Y, Ju X, Zou Z, Wang H, Jiang C (2012). Inhibition of autophagy ameliorates acute lung injury caused by avian influenza A H5N1 infection. *Sci Signal*, 5(212), ra16. doi: 10.1126/scisignal.2001931 [PubMed: 22355189]
- Takeshita F, Kobiyama K, Miyawaki A, Jounai N, & Okuda K (2008). The non-canonical role of Atg family members as suppressors of innate antiviral immune signaling. *Autophagy*, 4(1), 67–69. [PubMed: 17921696]
- Turabekova M, Rasulev B, Theodore M, Jackman J, Leszczynska D, & Leszczynski J (2014). Immunotoxicity of nanoparticles: a computational study suggests that CNTs and C60 fullerenes might be recognized as pathogens by Toll-like receptors. *Nanoscale*, 6(7), 3488–3495. doi: 10.1039/c3nr05772k [PubMed: 24548972]
- Varga ZT, Grant A, Manicassamy B, & Palese P (2012). Influenza virus protein PB1-F2 inhibits the induction of type I interferon by binding to MAVS and decreasing mitochondrial membrane potential. *J Virol*, 86(16), 8359–8366. doi: 10.1128/JVI.01122-12 [PubMed: 22674996]
- Villeret B, Dieu A, Straube M, Solhonne B, Miklavc P, Hamadi S, Garcia-Verdugo I (2018). Silver Nanoparticles Impair Retinoic Acid-Inducible Gene I-Mediated Mitochondrial Antiviral Immunity by Blocking the Autophagic Flux in Lung Epithelial Cells. *ACS Nano*, 12(2), 1188–1202. doi: 10.1021/acsnano.7b06934 [PubMed: 29357226]
- Walling BE, Kuang Z, Hao Y, Estrada D, Wood JD, Lian F, Lau GW (2013). Helical carbon nanotubes enhance the early immune response and inhibit macrophage-mediated phagocytosis of *Pseudomonas aeruginosa*. *PLoS One*, 8(11), e80283. doi: 10.1371/journal.pone.0080283 [PubMed: 24324555]
- Wang Y, Jiang K, Zhang Q, Meng S, & Ding C (2018). Autophagy in Negative-Strand RNA Virus Infection. [Review]. *Front Microbiol*, 9, 206. doi: 10.3389/fmicb.2018.00206 [PubMed: 29487586]
- Wu L, Zhang Y, Zhang C, Cui X, Zhai S, Liu Y, Yan B (2014). Tuning cell autophagy by diversifying carbon nanotube surface chemistry. *ACS Nano*, 8(3), 2087–2099. doi: 10.1021/nn500376w [PubMed: 24552177]
- Yatmaz S, Seow HJ, Gualano RC, Wong ZX, Stambas J, Selemidis S, Vlahos R (2013). Glutathione peroxidase-1 reduces influenza A virus-induced lung inflammation. *Am J Respir Cell Mol Biol*, 48(1), 17–26. doi: 10.1165/rcmb.2011-0345OC [PubMed: 23002098]
- Yeganeh B, Ghavami S, Rahim MN, Klonisch T, Halayko AJ, & Coombs KM (2018). Autophagy activation is required for influenza A virus-induced apoptosis and replication. *Biochim Biophys Acta Mol Cell Res*, 1865(2), 364–378. doi: 10.1016/j.bbamcr.2017.10.014 [PubMed: 29108912]
- Zamoiskii EA (1956). Evaluation of Reed-Muench method in determination of activity of biological preparations. *Zh Mikrobiol Epidemiol Immunobiol*, 27(1), 77–83.
- Zeinabadi HA, Zarrabian A, Saboury AA, Alizadeh AM, & Falahati M (2016). Interaction of single and multi wall carbon nanotubes with the biological systems: tau protein and PC12 cells as targets. *Sci Rep*, 6, 26508. doi: 10.1038/srep26508 [PubMed: 27216374]
- Zorov DB, Juhaszova M, & Sollott SJ (2014). Mitochondrial reactive oxygen species (ROS) and ROS-induced ROS release. *Physiol Rev*, 94(3), 909–950. doi: 10.1152/physrev.00026.2013 [PubMed: 24987008]
- Zorova LD, Popkov VA, Plotnikov EY, Silachev DN, Pevzner IB, Jankauskas SS, Zorov DB (2017). Mitochondrial membrane potential. *Anal Biochem*. doi: 10.1016/j.ab.2017.07.009

A.

HDR (nm)	Zeta Potential (mV)	EPM ($\times 10^{-8} \text{ m}^2\text{V}^{-1}\text{s}^{-1}$)
280.1 ± 201.5	-2.4 ± 0.6	-0.2 ± 0.1

B.

**Figure 1.**

SWCNT characterization and changes in cell viability. (A) The average hydrodynamic radius (HDR), zeta potential (ZP), and electrophoretic mobility (EPM) of SWCNTs in advanced RPMI 1640 media at 37 °C for 24 hours. (B) SAEC were exposed to different doses of SWCNTs for 24 hours and cell viability was determined by a trypan blue assay. A total of six samples per group were measured and data presented as Mean \pm SD. Asterisks “*” above each bar represent statistically significant differences compared to control ($P < 0.05$).

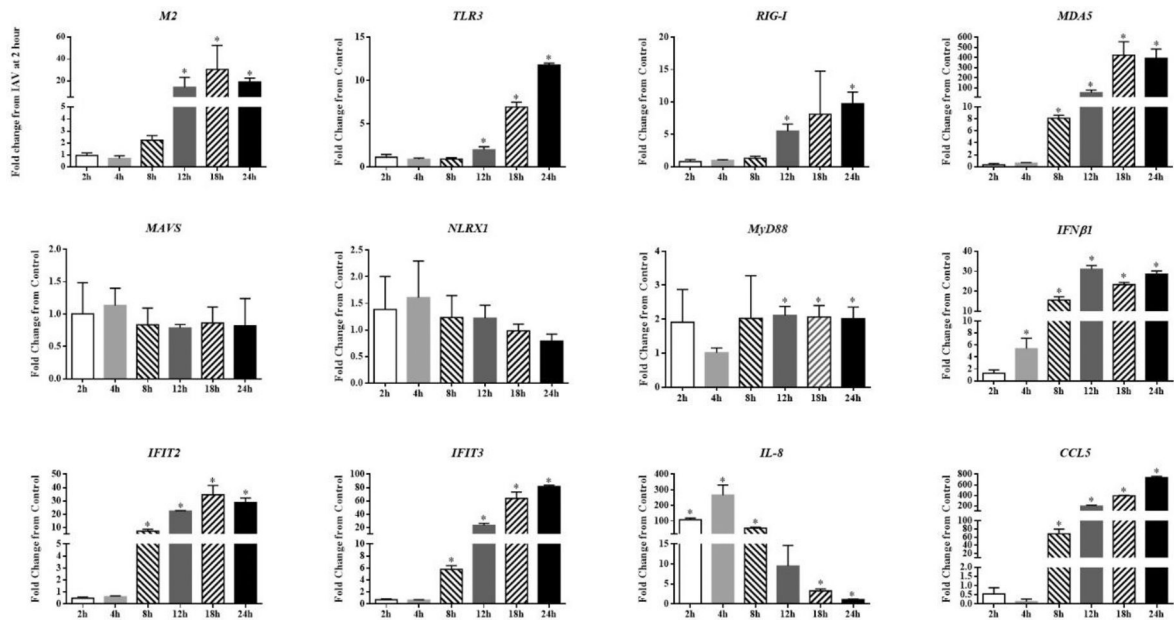


Figure 2.

Expression of immune genes in SAEC exposed to IAV over time. SAEC were exposed to IAV at MOI=0.5 for 2, 4, 8, 12, 18, and 24 hours. Cells were collected for RNA extraction and mRNA expression of immune genes were measured by qPCR. Fold change was calculated as IAV / control at each timepoint for all except *M2*. Fold change for *M2* was calculated as IAV at each timepoint / IAV 2 h. A total of six samples per group were measured and data presented as Mean \pm SD. Asterisks “*” above each bar represent statistically significant differences compared to IAV 2 h treatment ($P < 0.05$).

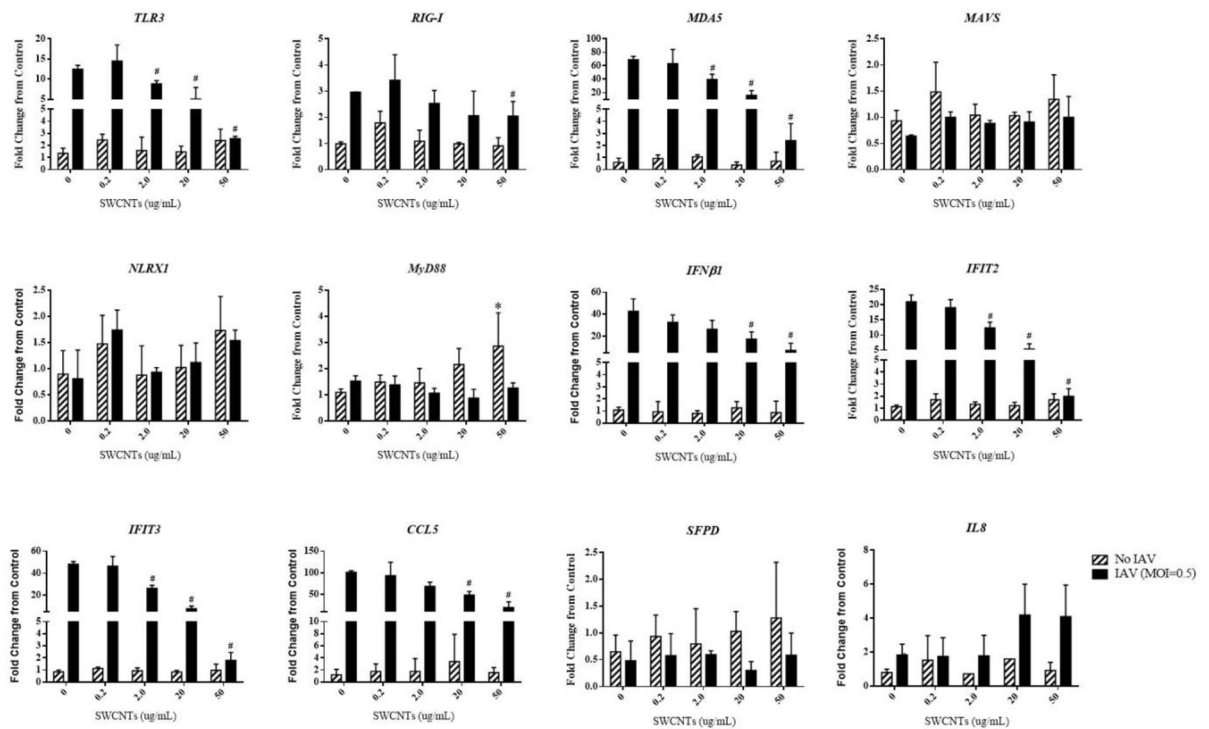


Figure 3.

Expression of immune genes in SAEC exposed to SWCNTs and IAV. SAEC were exposed to SWCNTs at different doses for 24 hours followed by IAV infection at MOI=0.5 for another 24 hours. Cells were collected for RNA extraction and mRNA expression of immune genes were measured by qPCR. A total of six samples per group were measured. The fold change from control (no IAV and no SWCNTs) were calculated and graphed as Mean \pm SD. Asterisks “***” above each bar represent statistically significant differences compared to control (hatched bars). Pound “#” indicates statistically significant differences compared to IAV only (black bars) ($P < 0.05$).

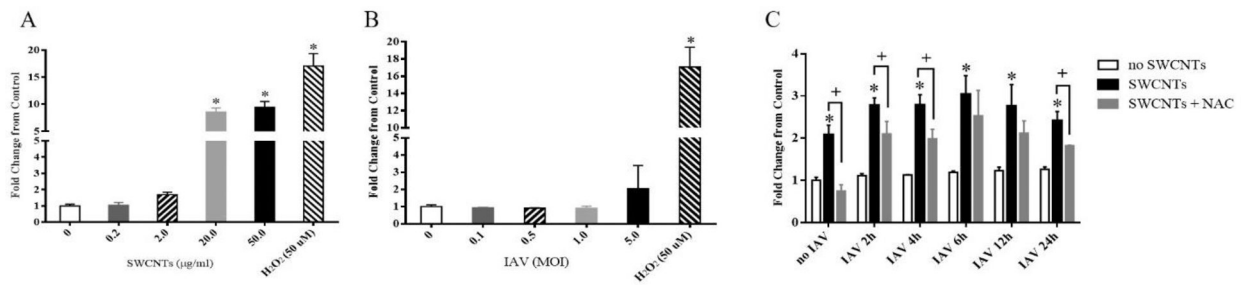


Figure 4.

Changes in ROS production induced by SWCNTs, IAV, and antioxidant NAC. A DCFDA method was used to determine the ROS production in SAEC exposed to different doses of SWCNTs (A), IAV (B), and cells exposed to SWCNTs (50 µg/mL) following time course of IAV (MOI=0.5) infection in the presence or absence of NAC (1 mM) (C). A total of six samples per group were measured and data presented as Mean ± SD. Asterisks “*” above each bar indicate statistical differences compared to control. Plus signs (+) represent statistically significant differences between SWCNTs + IAV and NAC + SWCNTs + IAV at each time point ($P < 0.05$).

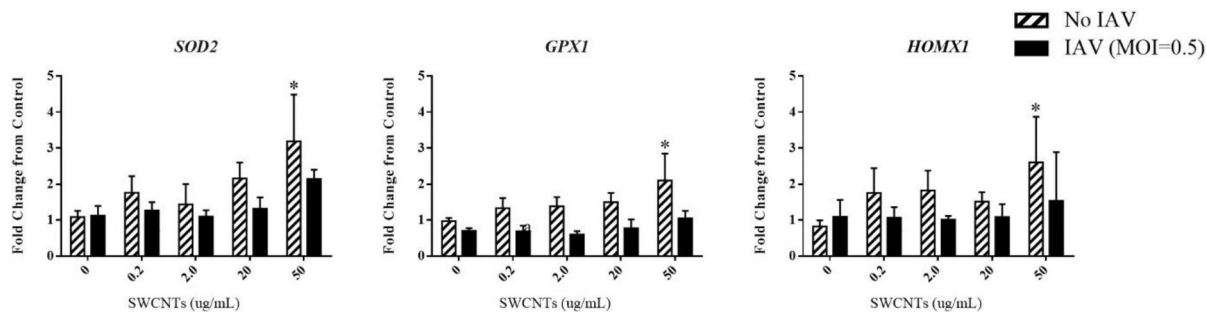
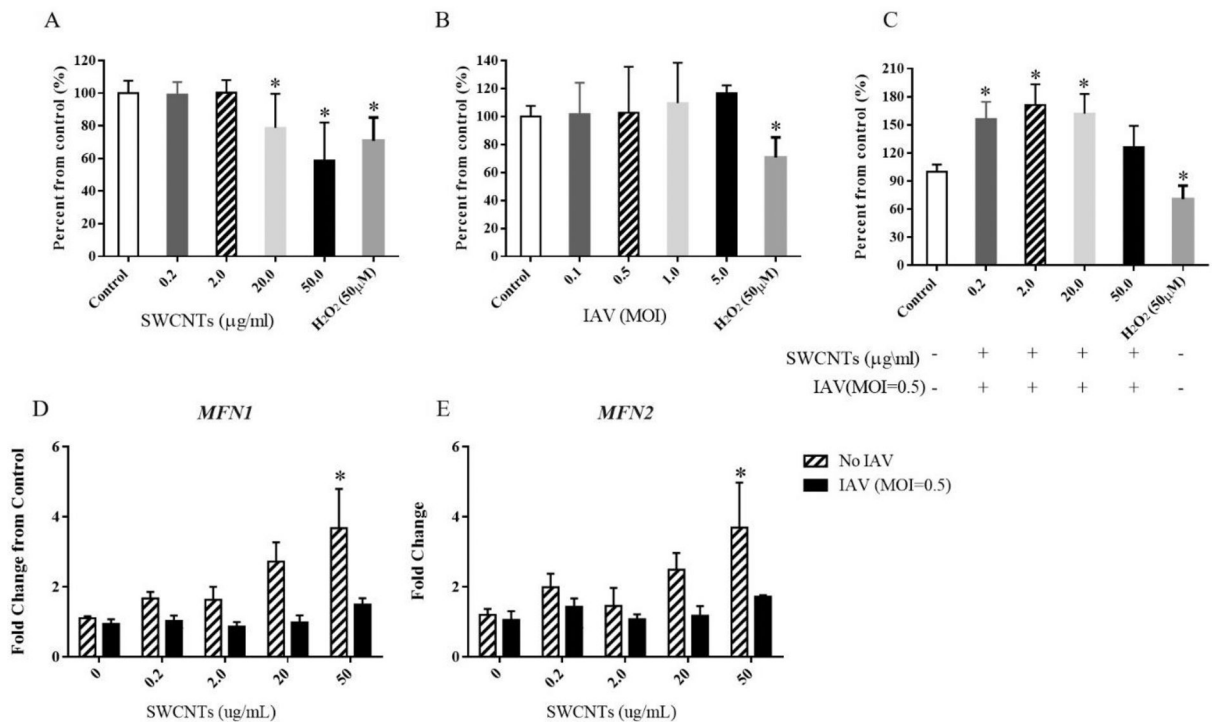


Figure 5.

Expression of oxidative stress-related genes in SAEC exposed to SWCNTs and IAV. SAEC were exposed to SWCNTs at different doses for 24 hours followed by IAV infection at MOI=0.5 for another 24 hours. Cells were collected for RNA extraction and mRNA expression of immune genes were measured by qPCR. A total of six samples per group were measured and data presented as Mean \pm SD. Asterisks “*” indicate statistically significant differences of SWCNT treated compared to control. ($P < 0.05$)

**Figure 6.**

Changes in mitochondrial membrane potential (MMP) and mRNA expression of mitofusin 1 and 2 (*MFN1* and *MFN2*) by SWCNTs and IAV. A TMRE method was used to determine the MMP in SAEC exposed to different doses of SWCNTs (A), IAV (B), and exposed to different doses of SWCNTs for 24 hours following IAV (MOI=0.5) infection for 24 hours (C). The mRNA expression of *MFN1* (D) and *MFN2* (E) were measured by qPCR in SAEC which were exposed to SWCNTs at different doses for 24 hours followed by IAV infection at MOI=0.5 for another 24 hours. A total of six samples per group were measured and data presented as Mean \pm SD. Asterisks “*” above each bar indicate statistically significant differences compared to control. ($P < 0.05$)

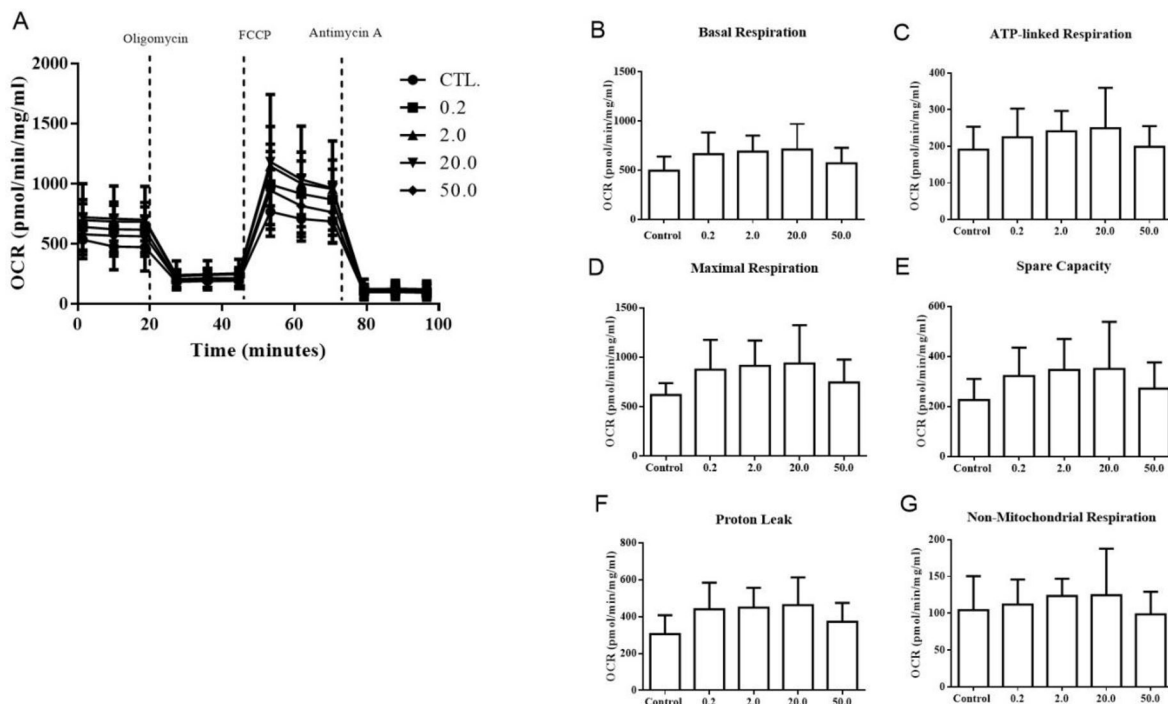


Figure 7.

Effects of SWCNTs on mitochondrial bioenergetics. A Seahorse assay was used to determine the oxygen consumption rate of SAEC exposed to different doses of SWCNTs for 24 hours. Overall oxygen consumption rate (A), basal respiration (B), ATP-linked respiration (C), maximal respiration (D), spare capacity (E), proton leak (F), and non-mitochondrial respiration (G) were measured and calculated. A total of six replicates per group were measured and data presented as Mean \pm SD.

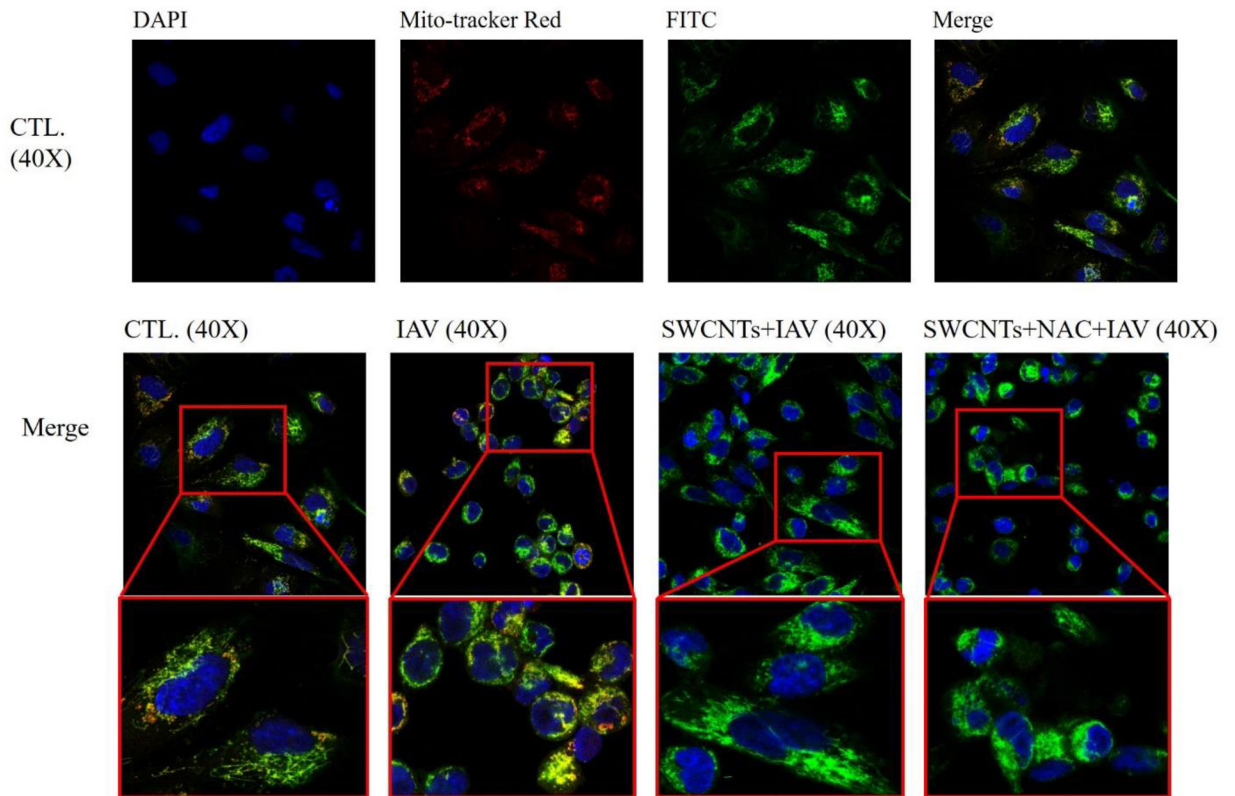


Figure 8.

Changes in MAVS colocalization in SAEC by SWCNTs, NAC, and IAV. SAEC were exposed to 50 $\mu\text{g}/\text{mL}$ SWCNTs for 24 hours, then NAC (1mM) for 2 hours, followed by IAV infection at MOI=0.5 for another 24 hours. Cells were fixed for immunofluorescence staining to visualize co-localization of mitochondria (mitotracker red), MAVS protein (Anti-MAVS FITC, green), and nucleus (DAPI, blue) as indicated by square in the figures.

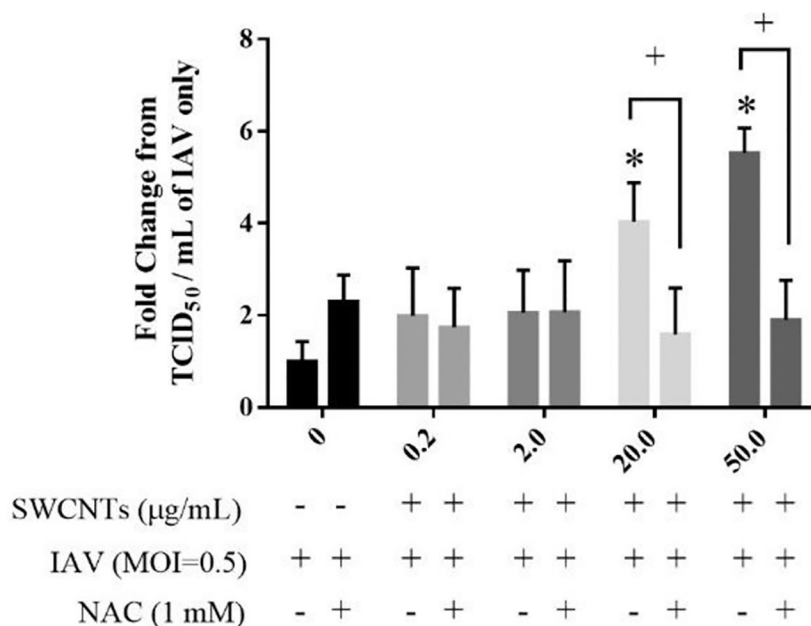


Figure 9. NAC significantly reduced SWCNT-increased IAV viral titer in SAEC. SAEC were exposed to different doses of SWCNTs (µg/ml) for 24 hours, followed by 2 hours of NAC treatment (1mM), and then IAV (MOI=0.5) challenge for another 24 hours. The supernatant of each treated well was collected for virus titer measurement by TCID₅₀ assay. A total of six samples per group were measured and data presented as Mean ± SD. Asterisks “*” above each bar indicate statistical differences compared to control. Plus symbols (+) above each bar represent statistically significant differences between SWCNTs + IAV and NAC + SWCNTs + IAV at each SWCNT dose ($P < 0.05$).

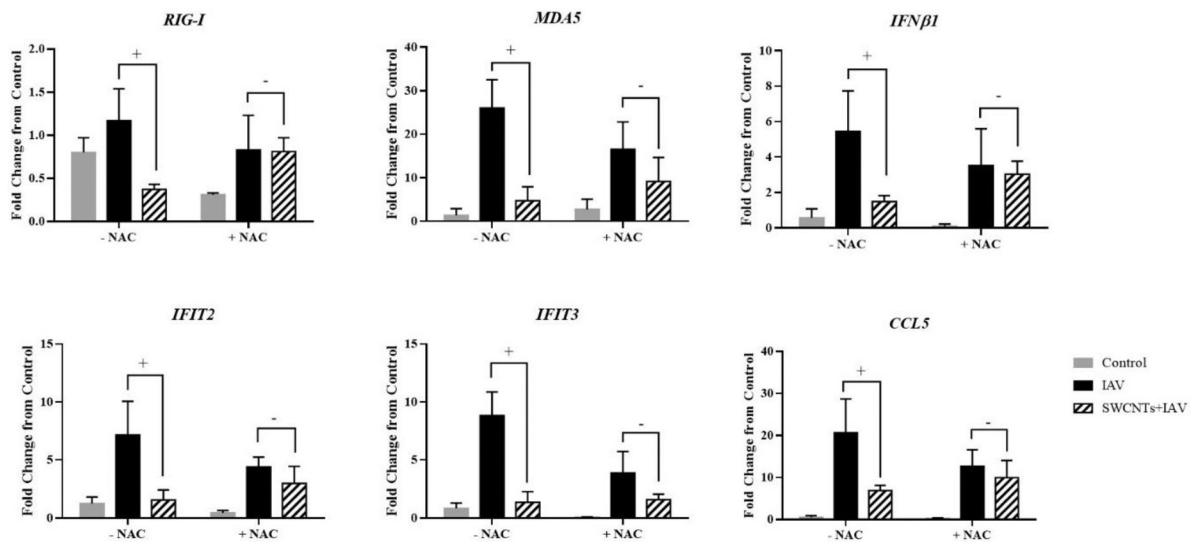


Figure 10.

NAC partially rescues SWCNT-inhibited antiviral gene expression in SAEC. SAEC were exposed to SWCNTs (20 $\mu\text{g}/\text{ml}$) for 24 hours, followed by 2 hours of NAC treatment (1mM), and then IAV (MOI=0.5) challenge for another 24 hours. Cells were collected for RNA extraction and mRNA expression of immune genes were measured by qPCR. A total of six samples per group were measured and data calculated as fold change from control and presented as Mean \pm SD. Plus signs (+) above each bar indicate statistically significant differences between IAV and SWCNTs + IAV while minus signs “-” represent no difference ($P < 0.05$).

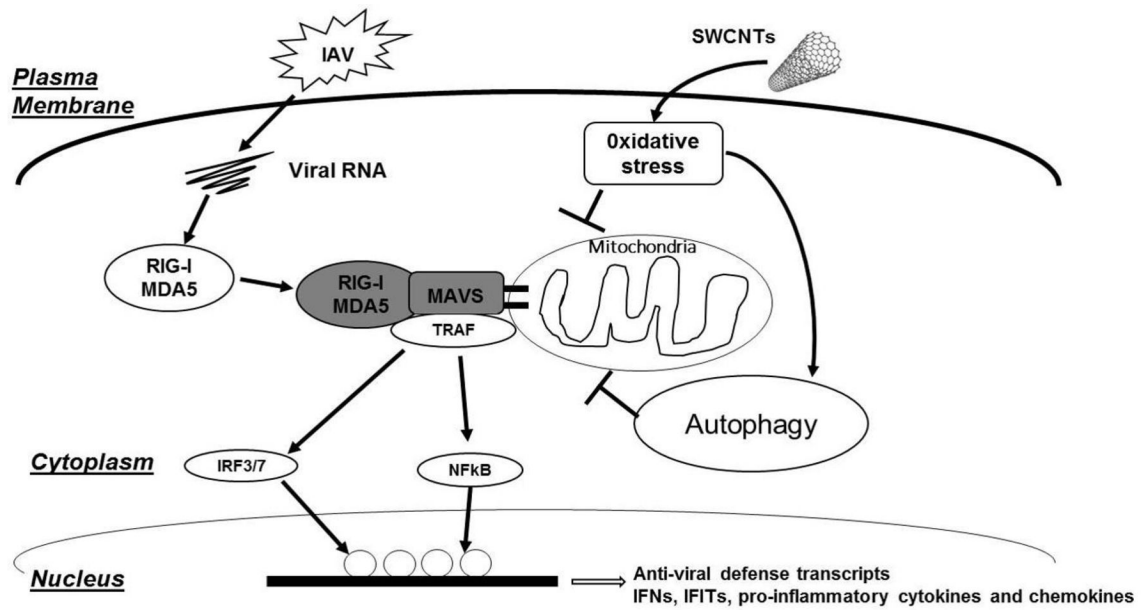


Figure 11. Schematic pathway showing how SWCNTs can impact IAV activation of the RLR/MAVS pathway through oxidative stress in lung epithelial cells.

Table 1.

Viral titers in cell media and expression of *M2* in SAEC exposed to SWCNTs and IAV. SAEC were exposed to SWCNTs at different doses for 24 hours followed IAV infection for another 24 hours. Cell culture media was pooled for each treatment to determine virus particle number by TCID₅₀ assay. Cells were collected for RNA extraction and mRNA expression of *M2* were measured by qPCR. A total of six samples per group were measured and data presented as Mean ± SD. Asterisks “*” represent statistically significant differences compared to IAV treatment ($P < 0.05$).

Treatment (SWCNT dose µg/mL)	Virus titer (TCID ₅₀ /mL)	Virus titer (Fold change from IAV)	IAV <i>M2</i> Expression (% change from IAV)
IAV	2.32E+05	-----	100.00 ± 84.83
0.2 SWCNTs + IAV	5.00E+05	2.2 X	69.15 ± 22.57
2.0 SWCNTs + IAV	3.15E+05	1.4 X	31.43 ± 12.05 *
20.0 SWCNTs + IAV	5.00E+05	2.2 X	22.08 ± 7.50 *
50.0 SWCNTs + IAV	7.92E+05	3.4 X	36.88 ± 19.09